

Rochester Institute of Technology

RIT Digital Institutional Repository

Theses

2003

A computational approach to arteriolar bifurcations: evaluation of factors influencing predicted wall shear stress

Charles Robinson

Follow this and additional works at: <https://repository.rit.edu/theses>

Recommended Citation

Robinson, Charles, "A computational approach to arteriolar bifurcations: evaluation of factors influencing predicted wall shear stress" (2003). Thesis. Rochester Institute of Technology. Accessed from

This Thesis is brought to you for free and open access by the RIT Libraries. For more information, please contact repository@rit.edu.

A Computational Approach to Arteriolar Bifurcations: Evaluation of Factors Influencing Predicted Wall Shear Stress

by

Charles L. Robinson

**A Thesis Submitted in
Partial Fulfillment of the
Requirement for the**

**MASTER OF SCIENCE
IN
MECHANICAL ENGINEERING**

Approved by:

Dr. Risa Robinson
Department of Mechanical Engineering

(Thesis Advisor)

Dr. Harvey Palmer
Dean, School of Engineering

Dr. Mark Kempski
Department of Mechanical Engineering

Dr. Edward C. Hensel
Department Head, Mechanical Engineering

**DEPARTMENT OF MECHANICAL ENGINEERING
ROCHESTER INSTITUTE OF TECHNOLOGY**

November, 2003

Permission from author required

A Computational Approach to Arteriolar Bifurcations: Evaluation of Factors Influencing Predicted Wall Shear Stress

I, *Charles L Robinson*, prefer to be contacted each time a request for reproduction is made. If permission is granted, any reproduction will not be for commercial use or profit. I can be reached at the following address:

Date: 12/11/03

Signature of Author: Charles L. Robinson

Table Of Contents

Figures and Tables.....	i
Abstract.....	iii
Chapter 1: Introduction.....	4
1.1 Understanding Circulation.....	4
1.2 Hemodynamics.....	6
1.2.1 The Microcirculatory Vessel Geometry.....	6
1.2.2 Rheological Properties of Blood.....	8
1.3 Blood Flow Analysis in Microcirculation.....	11
1.3.1 Defining Properties.....	11
1.3.2 Analysis Methods.....	14
Chapter 2: Computational Model Development.....	17
2.1 The Physical Model.....	17
2.2 Governing Equations.....	23
2.3 FIDAP Analysis.....	24
2.3.1 Volume Of Fill (VOF).....	24
2.3.2 FIDAP FEM Formulation.....	27
2.4 Analysis Concerns.....	29
Chapter 3: Wall Shear Stress Analysis.....	31
3.1 Computational Validation.....	31
3.1.1 Comparison of Two-Dimensional Results to Three-Dimensional Results	31
3.1.2 Wall Shear Stress Comparisons to Published Studies in Golden Hamsters	35
3.2 Influence of Corner Geometry.....	38
3.3 Red Blood Cell Presence.....	51
3.3.1 Droplet Presence in a Straight Vessel.....	52
3.3.2 Analysis of Droplet Property Values in a 30 Degree Bifurcation.....	53
3.3.3 Qualification of Droplet Property Values	57

3.3.4	Droplet Presence in a Bifurcation.....	60
3.3.5	Multiple Droplets in a Flow.....	64
Chapter 4: Future Developments.....		68
4.1	Appropriateness of Study Simplifications.....	68
4.1.1	2-D Simplification.....	69
4.1.2	Volume of Fluid.....	69
4.2	Multiple Particle Flow.....	70
4.3	Three Dimensional Model.....	70
REFERENCES.....		71
A1	Newtonian Flow, Corner Geometry Analysis, Bifurcation Size.....	74
A2	Analysis Shortcomings, Guideline for Continuation of Research.....	75

Figures and Tables

Chapter 1 Introduction

Figure 1.1: The Human Circulatory System	5
Figure 1.2: Microcirculatory Vessel	6
Figure 1.3: Typical Bifurcation Geometry.....	7
Figure 1.4: Hematocytes	8
Figure 1.5: Red Blood Cell	9
Table 1.1: Properties of Blood and Red Blood Cells	10
Figure 1.6: Whole Blood Viscosity Approximation.....	12

Chapter 2: Computational Model Development

Figure 2.1: Typical Transverse Arteriole.....	18
Figure 2.2: Bifurcation Geometry.....	19
Figure 2.3: Nominal Endothelial Cell Location.....	20
Figure 2.4: Quadrilateral Elements.....	21
Figure 2.5: Particle Model Definition.....	23
Figure 2.6 Fractional Fill Diagram.....	25
Figure 2.7: Surface Tension of a Spherical Droplet.....	26

Chapter 3: Wall Shear Stress Analysis

Figure 3.1: 2D-3D Wall Shear Stress Comparison, 30 degree Bifurcation.....	33
Figure 3.2: 2D-3D Wall Shear Stress Comparison, 90 degree Bifurcation.....	34
Figure 3.3: 2D-3D Wall Shear Stress Comparison, 150 degree Bifurcation.....	34
Figure 3.4: 2-D Comparison to Published In Vivo and In Vitro Data, 30 Degree Bifurcation.....	37
Figure 3.5: 2-D Comparison to Published In Vivo and In Vitro Data, 90 Degree Bifurcation.....	37
Figure 3.6: 2-D Comparison to Published In Vivo and In Vitro Data, 150 Degree Bifurcation.....	38
Figure 3.7: Characteristic “s” Shape in Bifurcation Wall Shear Stress.....	39

Figure 3.8a: Upper Front Wall Shear Stress, 30 degree Bifurcation.....41

Figure 3.8b: Upper Front Wall Shear Stress, 30 degree Bifurcation.....42

Figure 3.9: Upper Front Wall Shear Stress, 90 degree Bifurcation.....42

Figure 3.10a: Upper Front Wall Shear Stress, 150 degree Bifurcation.....43

Figure 3.10b: Upper Front Wall Shear Stress, 150 degree Bifurcation.....43

Figure 3.11a: Upper Back Wall Shear Stress, 30 degree Bifurcation.....45

Figure 3.11b: Upper Back Wall Shear Stress, 30 degree Bifurcation.....45

Figure 3.12: Upper Back Wall Shear Stress, 90 degree Bifurcation.....46

Figure 3.13a: Upper Back Wall Shear Stress, 150 degree Bifurcation.....46

Figure 3.13b: Upper Back Wall Shear Stress, 150 degree Bifurcation.....47

Figure 3.14a: Lower Wall Shear Stress, 30 degree Bifurcation.....48

Figure 3.14b: Lower Wall Shear Stress, 30 degree Bifurcation.....49

Figure 3.15: Lower Wall Shear Stress, 90 degree Bifurcation.....49

Figure 3.16a: Lower Wall Shear Stress, 150 degree Bifurcation.....50

Figure 3.16b: Lower Wall Shear Stress, 150 degree Bifurcation.....50

Figure 3.17: Wall Shear Stress, Droplet Flow.....53

Figure 3.18a-e: Droplet Behavior with Changing Viscosity.....55

Figure 3.19a-e: Droplet Behavior with Changing Surface Tension56

Figure 3.20: Wall Shear Stress Dependency on Droplet Viscosity.....58

Figure 3.21: Wall Shear Stress Dependency on Surface Tension.....59

Figure 3.22: Bifurcation Geometry with Droplet Position.....60

Figure 3.23: Droplet Presence in a Bifurcation, Upper Front Wall Normalized Wall Shear Stress.....61

Figure 3.24: Droplet Presence in a Bifurcation, Upper Back Wall Normalized Wall Shear Stress.....62

Figure 3.25: Droplet Presence in a Bifurcation, Lower Wall Normalized Wall Shear Stress.....63

Figure 3.26: Multiple Droplets in Straight Vessel, Normalized Wall Shear Stress.....65

ABSTRACT

Recent studies of blood flow regulation at the microcirculatory level have linked the physical characteristics of the arteriolar bifurcations and the physiology of the flow through them to the autoregulatory mechanisms exhibited by the endothelial cell lining. Research in this area is decomposed to the following two components: understanding the biochemical activity that takes place at the cellular level as a result of flow-induced stimulation and characterizing the physical flow behavior causing the stimulation. The following study develops the currently accepted method of characterizing the physical flow behavior, in the form of wall shear stress, through computational analysis.

The goal of this research was to improve the computational methodology used for arterial blood flow analysis to predict and characterize wall shear stress. In doing so, all factors introduced by the modeling techniques were analyzed for influence on predicted wall shear stress in order to prove the credibility of the methodology. This process also extended to a characterization of wall shear stress effects as a result of changing model geometry and the physical composition of the blood as a particle-laden fluid, which better represent the physical features of these microcirculatory vessels.

The thoughts presented in this thesis corresponding to the development and proof of a revised approach for wall shear stress prediction in arteriolar bifurcations provide a consistent method for the development and evaluation of single factors of the realistic model as they relate to wall shear stress. The goal of this approach was to simplify the computational problem into its constituents and evaluate the wall shear stress influence of each on a singular basis.

Chapter 1

Introduction

Similar to the development of medical breakthroughs like artificial organs, which is led by research dedicated to arterial blood flow, Microvascular research, or the study of the microcirculation, is a growing area of interest, which may lead to improvements in medical treatment. Investigation of the physical mechanisms in microcirculation is expected to lead to the prevention of atherosclerotic diseases, which hinder or block blood flow (Taylor, 2000). In addition, research will lead to improved medication techniques used by physicians for treatment purposes. One area of Microcirculation is focused on the study of metabolic responses of arteriolar vessels that are triggered by wall shear stress (Frame and Sarelius, 1993; Cassotet al., 1998). This research will further evaluate the dynamics of blood flow through microcirculatory vessels with a characterization of wall shear stress.

One area of microvascular research is concentrated on quantifying blood flow effects on a local level. The dynamic and physical properties of the blood flow are strongly correlated to regulation mechanisms of the body (Frame and Sarelius, 1993; Cassotet al., 1998). Regions of expected flow changes, such as bifurcations, are of great interest since they may serve as “switchpoints” for flow regulation (Frame and Sarelius, 1993). Greater understanding of microcirculation will also give more understanding of cell transport; flow phenomena and mechanical interactions (Popel and Pittman, 2000).

1.1

Understanding Circulation

To understand microcirculation, an understanding of the circulatory system as a whole is needed (Fig. 1.1). The circulation system is responsible for transporting oxygen and nutrients

to individual cells throughout the entire body via blood. A complex network of blood vessels, known as arterial vessels, carry the oxygen and nutrient-rich blood from the heart to every tissue composing the body. To do this, the larger vessels known as arteries, branch, or split, into smaller arteriole vessels, which then branch into the smallest capillary vessels. Cells may then absorb oxygen and nutrients from the blood through the capillary vessel walls, which consist of a single endothelial cell layer.

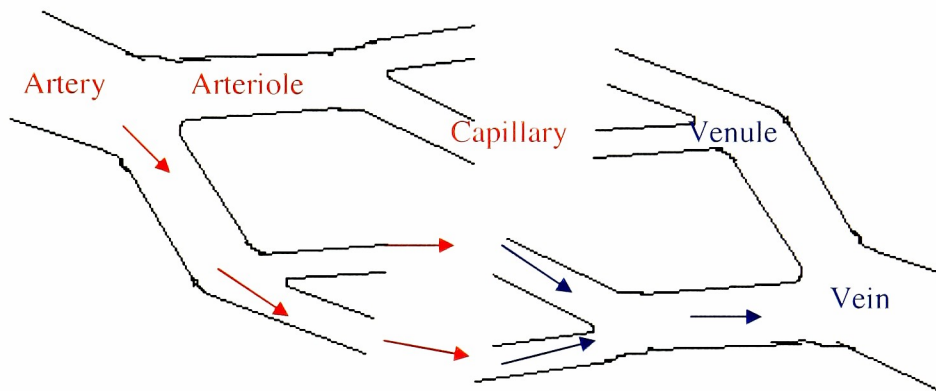


Figure 1.1: The Human Circulatory System

The blood continues to flow through the capillary vessels and enters the seemingly similar venous network consisting of small venules, which converge into larger veins, serving to carry the nutrient and oxygen-deprived blood back to the heart, thereby closing the circulatory loop.

The systemic microcirculatory system in a human contains more than 40 percent of the entire pulmonary volume of the circulatory system (Schneck, 2000). There are nearly 18.5 million arterioles as large as 100 μm in diameter, 239 million metarterioles ranging

from 25 μm to 10 μm in diameter, and more than 16 billion capillaries ranging from 10 μm to 3 μm in diameter (Schneck, 2000). Aside from their small size, a major distinction of microcirculatory vessels, shown in Figure 1.2, is their thin walls that allow for the diffusion of substances within the blood to the surrounding cells or from the surrounding cells to the blood.

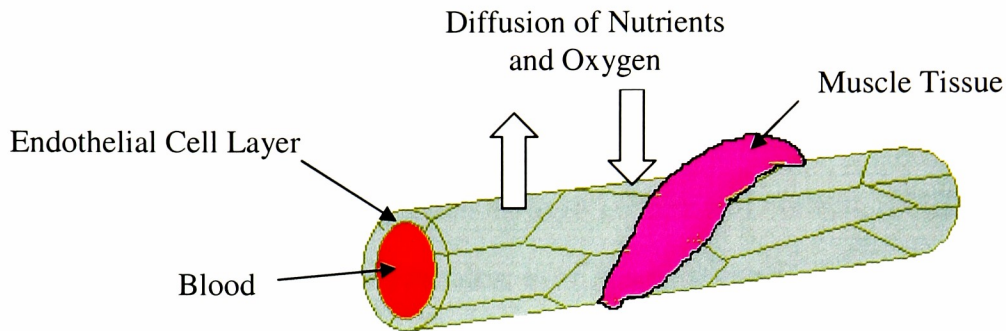


Figure 1.2: Microcirculatory Vessel

1.2 Hemodynamics

An equally important part of the circulation is the blood that flows through the vessel network and its characteristics. Blood flow dynamics, or hemodynamics, depend on both the geometric characteristics of the circulatory vessels and the rheological, or constitutive, properties of the blood.

1.2.1 The Microcirculatory Vessel Geometry

A systemic microcirculatory system is composed of numerous arteriole and capillary vessels, the smallest of which, are on the order of 10 μm in diameter. Unlike the larger vessels of the arterial system, very little vascular smooth muscle tissue surrounds the vessels of the

microcirculation. Nevertheless, the muscle tissue enables the vessels to contract and expand to changes in flow rate (shear rate) as a mechanism of the control of blood flow to a tissue. This response is known as the myogenic response, which is a contraction of a vessel due to an increase in flow rate or a dilation of a vessel due to a decrease in flow, which maintains constant flow shear (Popel and Pittman, 2000). It's within these biological responses that a greater understanding of the body's autoregulation of blood flow to tissues will emerge. As shown in Figure 1.2, the inner arteriole and capillary vessel wall is composed of a single layer of endothelial cells that respond chemically via vasoactive substances to shear sensations from the blood flow within the vessel (Popel and Pittman, 2000).

Vessel bifurcations, or junctions, exist in a wide range of orientations throughout the microvascular networks and are typically classified as either a Y-type or a T-type bifurcation depending upon the bifurcation angle (Figure 1.3). The bifurcation angle is the angle the branching vessel makes with the parent vessel. A bifurcation angle of 90 degrees is known as a T-type bifurcation.

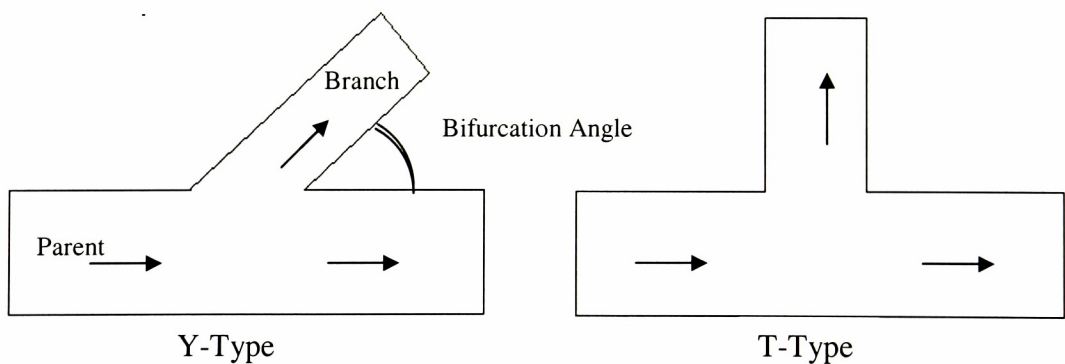


Figure 1.3: Typical Bifurcation Geometry

For the purposes of understanding blood flow behavior through bifurcating vessels, a diameter ratio and flow rate ratio of the branch vessel to the parent vessel are particularly important.

1.2.2 Rheological Properties of Blood

Whole blood consists of a fluid substance called plasma in which relatively large particles, or hematocytes, are suspended. The hematocytes found in the blood consist of leukocytes, thrombocytes, and erythrocytes, commonly known as white blood cells, platelets, and red blood cells, respectively, with sizes ranging from 2-10 micrometers in equivalent diameter (Fig 1.4).

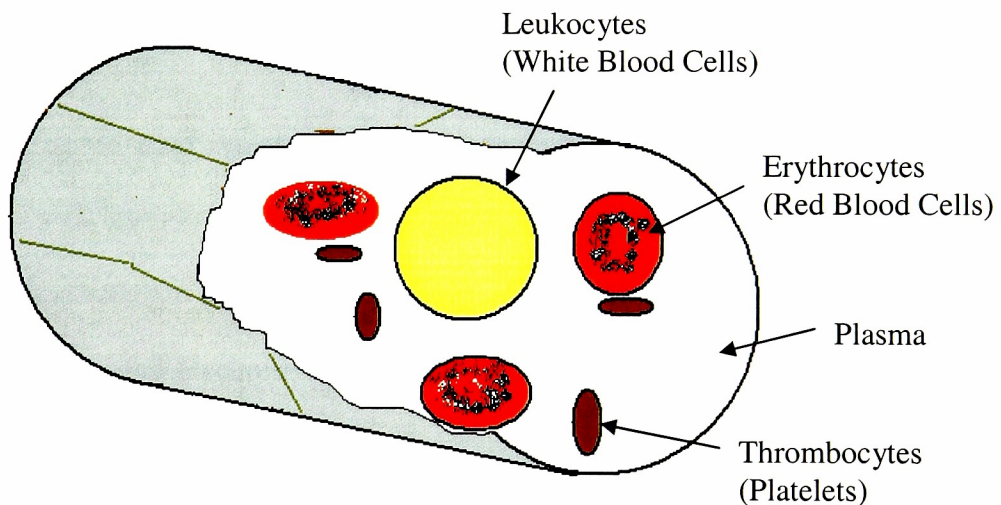


Figure 1.4: Hematocytes

Plasma represents the fluid by which the white blood cells, platelets, and red blood cells are transported. The fluid properties of plasma (density and viscosity) have been

obtained experimentally and are well known. It has been shown through viscometer measurements that plasma behaves as a Newtonian fluid (Schneck, 2000).

White blood cells are the largest of the hematocytes found in blood and aid in the body's defense against sickness (Fig. 1.5). Slightly larger in size than red blood cells with a mean diameter of $8.5 \mu\text{m}$, white blood cells maintain a more spherical shape and are far less deformable than red blood cells (Waugh and Hochmuth, 2000). The presence of these cells in blood is nearly 700 times lower than that of red blood cells (Schneck, 2000). These particles exhibit cortical tension characteristics that preserve a rigid spherical shape for the cell while in the bloodstream.

Platelets are the smallest particles found in the blood. Having an elongated spherical shape, platelets are nearly one-fourth the size of red blood cells (Schneck, 2000). Platelets are more numerous than white blood cells and play a critical role in the blood clotting process.

By far the most abundant of the hematocytes are the red blood cells, RBC's, which serve as oxygen carriers. Red blood cells are significantly more deformable than white blood cells. These disk-like particles have a mean diameter of $8 \mu\text{m}$ in human blood and are very flexible (Waugh and Hochmuth, 2000; Evans and Yeung, 1989). Figure 1.5 presents the geometry of a typical red blood cell.

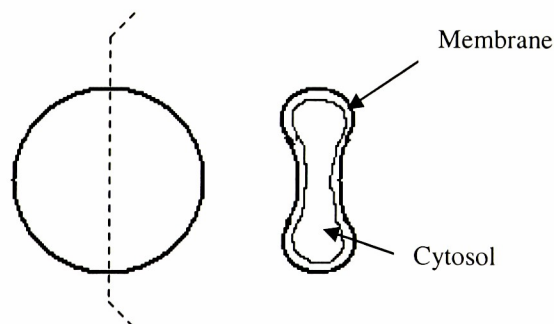


Figure 1.5: Red Blood Cell

Structurally, red blood cells consist of a Newtonian fluid substance known as cytosol enclosed in a thin, elastic membrane. The cytosol contains hemoglobin, which carries oxygen. The membrane is characterized mechanically by several elastic properties: shear modulus, bending stiffness, and an area expansivity modulus. It is the membrane that gives the red blood cell its distinct disk shape and its deformability behavior.

In the interest of developing an accurate characterization of blood flow in arterioles, it is necessary to understand and consider how erythrocytes may influence flow behavior.

Table 1.1 represents a compilation of research of known rheological properties of blood.

Rheological Properties

References	Red Blood Cell										Plasma			Whole Blood			
	Mean Diameter (m)	Membrane					Cytosol					Surface Tension (N/m)	Viscosity (N*s/m ²)	Density (kg/m ³)	Surface Tension (N/m)	Viscosity (N*s/m ²)	Density (kg/m ³)
		Area Expansivity Modulus, K (N/m)	Shear Modulus, μ (N/m)	Bending Stiffness (J)	Surface Tension (N/m)	Viscosity (N*s/m ²)	Density (kg/m ³)	Surface Tension (N/m)	Viscosity (N*s/m ²)	Density (kg/m ³)							
Hochmuth (2000)		0.5	6 E -06 - 9 E -06		30 E -06 (WBC)												
Evans et al. (1976)		0.5	5 E -06														
Hochmuth (1987)				1 E -19		0.6 E -06 - 1.2 E -06											
Evans and Yeung (1989)	8 E -06 (WBC)				35 E -06 (WBC)												
Evans and Waugh (1979)		0.45	6.6 E -06														
Katnik and Waugh (1990)		0.5															
Barbenel (1981)									0.00427							0.005	
Harkness (1971)													0.00116 - 0.00135				
Schneck (2000)	7.5 E -06									1098		0.0015 - 0.002	1035		0.003 - 0.006	1057	
Waugh and Hochmuth (2000)		0.48	6 E -06	2 E -19		36 E -07											
Waugh and Hochmuth (2000)									0.0042								
Waugh and Evans (1979)		0.4	5.8 E -06														

Note: All Values Referenced for Temperature of 37 degrees Celcius and Hematocrit of 44%

Table 1.1: Properties of Blood and Red Blood Cells

1.3

Blood Flow Analysis in Microcirculation

Blood flow behavior in the microcirculation depends not only on the geometric characteristics of the arteriole vessels, but also the constitutive, or rheological, properties of the blood (Lipowsky, 1987). It is therefore necessary to understand how local vessel geometry and flow composition influence the flow characteristics which are then integrated within a communication cycle for the regulation of blood flow within a microvascular network (Fox and Frame, 2002). While the most recent studies by Dr. Molly Frame (Biomedical Engineering, State University of New York at Stony Brook, Stony Brook, NY, 11794) investigate the involvement of endothelial cell intercommunication for flow regulation in the Hamster cremaster muscle, the current study is focused on providing quantifiable results of the vessel geometry and blood composition influence on the physical stresses experienced by the endothelial cell lining.

1.3.1

Defining Properties

For purposes of flow analysis, the viscous properties of a fluid are important to understand flow behavior. With this in mind, there are three ways that whole blood may be characterized: as (1) a homogenous, Newtonian fluid, classified with a relative viscosity, (2) a shear-thinning fluid, classified with a flow shear dependent relative viscosity, or (3) a particle-laden fluid with distinct property characteristics. In any case, Hematocrit (red blood cell volume fraction), vessel size (diameter), and relative viscosity, when considered

together, give a good understanding of true blood properties and correspondingly, flow behavior (Pries et al., 1990).

Typically, mathematical analysis of arterial blood flow, or macrocirculation, assume that whole blood is a fluid with a viscosity that increases with hematocrit (cellular concentration). However, to be more precise, whole blood should be modeled as a shear thinning fluid, where relative viscosity is based on hematocrit and also varies with characteristic flow shear. Although both methods are common and accepted practice for investigations entailing the macrocirculation, analysis of the microcirculation may not take advantage of the same viscosity approximations due to the relative size of the particles (cells) in the flow compared to the diameter of the vessels.

Both the Newtonian model and shear-thinning model approximate the viscosity of blood and its contents (RBC's). The relative size ratio between vessel diameter and a red blood cell is much larger in the macrocirculation than within the microvascular structure (See Fig. 1.6).

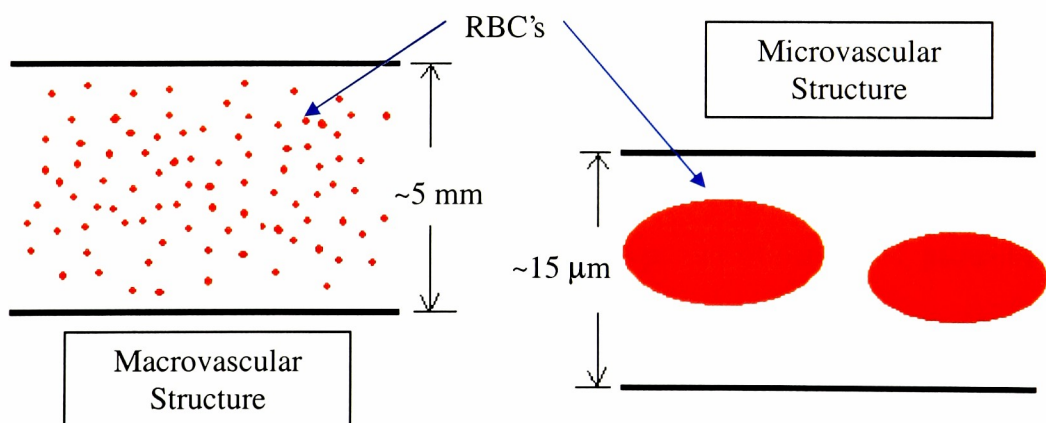


Figure 1.6: Whole Blood Viscosity Approximation

Additionally, in the microcirculation, since the vessel wall is in contact with the surrounding fluid plasma, whole blood is more accurately modeled as a particle-laden fluid. To substantiate this finding, two observable characteristics of blood flow in the microcirculation, the Fahraeus effect and the Fahraeus-Lindqvist effect are considered. Noticeable in microcirculatory blood flow is the Fahraeus effect, which is the concentration of RBC's in the center of the vessel, which causes a decrease in the Hematocrit between the branch and feed (Popel and Pittman, 2000). Additionally, the concentration of RBC's in the vessel center results in an apparent (near wall) viscosity that is lower than the bulk viscosity (Popel and Pittman, 2000). This observation is known as the Fahraeus-Lindqvist effect. Neither the Fahraeus effect nor the Fahraeus-Lindqvist effects may be duplicated using the Newtonian and shear-thinning methods.

For the laminar flow of a Newtonian fluid over a surface, wall shear stress serves as a single quantity by which to describe and compare local and spatial microcirculatory behavior (Lipowsky, 1987; Noren, 1999). Wall shear stress, defined by Equation 1.1, relates the shear stress on a surface to the product of the adjacent fluid viscosity and velocity profile gradient, also know as the shear rate.

$$\tau = \mu \frac{dU}{dy} \quad \text{[Equation 1.1]}$$

The wall shear stress reflects the effects of all local properties of the vessel, geometric and rheological; the vessel diameter, flow velocity, and fluid properties. It should be noted that the wall shear rate is also used to show and compare results of microvascular experiments. As a result of the direct contact of blood plasma with the vessel wall, the viscosity of blood plasma is instrumental to predicting wall shear stress throughout a capillary bifurcation, since

it, by the very definition of wall shear stress given by Equation 1.1, is a proportionality factor between shear stress, τ , and the shear rate, $\frac{dU}{dy}$.

1.3.2 Analysis Methods

Currently, *in vivo*, *in vitro*, and mathematical simulations represent three different approaches to obtaining detailed information about the flow characteristics of microcirculation. *In vivo* investigations are aimed at measuring flow properties directly from live vessels, typically in animals. These experiments, although limited in accuracy by imaging capabilities, provide a basis for understanding microcirculatory characteristics. Experiments using fabricated equipment to mimic microcirculatory flow behavior are known as *in vitro* experiments. These investigations allow greater control over flow variables, however, at the expense of introducing experimental error. Like *in vivo* experiments, *in vitro* experiments are also limited by the accuracy of measurement devices. Provided each flow mechanism may be explained numerically, mathematical experiments offer the capability of duplicating the entire flow behavior with much more detail than the other two types of investigation techniques. Numerical experiments are limited by the development of mathematical expressions and computational resources.

In Vivo

The largest area of experiments, *in vivo* studies of microcirculatory flow behavior in animals have explored regulatory mechanisms present in microcirculation. In most cases, fluorescent dye is injected into the blood to highlight the hematocytes in the flow. Advanced imaging techniques like Particle Image Velocimetry (PIV) are then used to observe and

record the characteristics of the blood flow. Interpretation of the particle locations and velocities from the images are used to develop characteristic velocity profiles within the vessels, from which the mechanical signature is obtained.

In the Hamster cremastor muscle, the spatial organization of common transverse arteriole networks has been shown to influence Hematocrit in different areas of the network, an observation known as phase separation (Frame and Sarelius, 1993). Furthermore, chemical induced stimulation of these common arteriole networks triggers metabolic responses which proves the existence of communication through endothelial cells lining the vessel walls, thus revealing their role in the autoregulation process (Frame and Sarelius, 1996). Most recently, localized wall shear stress in a downstream branch of common arteriole networks in the Hamster cremator muscle has been shown to effect flow regulatory responses at the network entry (¹Fox and Frame, 2002; ²Fox and Frame, 2002). In the microvascular networks of Winter frogs cinemicrography was used to correlate the interaction and radial displacement of erythrocytes with vessel size and flow velocity (Lominadze and Mchedlishvili, 1999). Other *in vivo* experiments used intravital microscopy to observe the influence of a macromolecular layer lining endothelial cells, glycocalyx, on flow resistance in the microcirculation of rats (Pries et al., 1997).

In Vitro

Using similar particle highlighting techniques to that used *in vivo*, the flow characteristics in D-shaped microchannels with and without an endothelial cell lining was examined to determine the influence of the bulging nucleus on wall shear stress (Frame et al., 1998). In another study, the pressure gradient in the vicinity of the bifurcation was found to increase when a glycerin test fluid with large flexible disks, representative of RBC's, was

used compared to when a glycerin test fluid without disks was used (Kiani and Cokelet, 1994).

Numerical

With the application of lubrication theory, the flow of a linearly elastic erythrocyte suspended in a linearly viscous fluid through a rigid tube with and without a glycocalyx lining showed a three-fold increase in flow resistance when glycocalyx was present (Damiano, 1998). Pulsatile flow in an arterial bifurcation displayed the influence of wall compliance on wall shear stress and showed a decrease in wall shear stress in the compliant wall model compared to the rigid wall model (Zhao et al., 2000). Numerical analysis of Newtonian flow through arterial bifurcations with rigid walls characterized the influence of bifurcation angle, branch diameter ratio, and entrance flow rate on separation regions in the flow field (Misra et al., 1993).

While each method of analysis has developed substantial information about microcirculatory blood flow, results using one method are compared with results from a different method to establish analysis credibility and information accuracy. The results and conclusions of this thesis are compared with the comparisons made between *in vivo* and computationally predicted values of wall shear stress within the Hamster cremaster muscle presented by Noren (1999) to establish credibility and accuracy.

Chapter 2

Computational Model Development

This chapter explains how the *in vivo* arteriole bifurcation is decomposed into a simplified and workable computational model. Specific details on the computational model development and methodology using Gambit 2.0, a pre-processing software for computational fluid dynamics (CFD), and the solution of the fluid flow equations using FIDAP 8.6.2, an analysis software for CFD, are given to support future advancements of this research.

As mentioned, the process of developing the computational model, or pre-processing, is the first step to performing a computational fluid dynamics analysis. Dimensional relationships, continuum definition via a computational grid, and physical and continuum properties are described. The computational analysis is set-up and performed in the next step that involves the application of the fluid flow equations to the continuum grid via discretization. The convergence of the equations represents the solution of the analysis, which may be queried for specific values or properties in the continuum domain. This is the final step of a complete computational fluid dynamics analysis known as post-processing.

2.1

The Physical Model

The microvascular geometry of common arteriole bifurcations, as described in section 1.2.1, are typical of the common transverse arteriole (Fig. 2.1) found in the Hamster cremaster muscle (Frame and Sarelius, 1993).

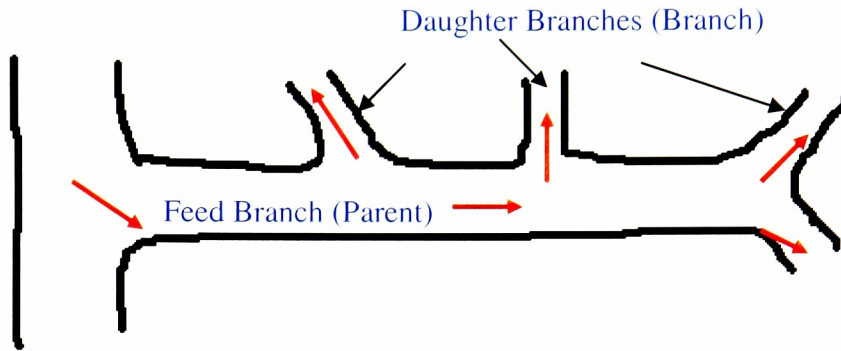


Figure 2.1: Typical Transverse Arteriole

The *in vivo* arteriole vessels of interest were studied as simple, non-compliant (rigid-walled), two-dimensional flow geometries. Two types of models, bifurcation models and straight channel models, were then developed for studying corner geometry effect and the effect of the particulate nature of blood on wall shear stress.

Bifurcation models with angles of 30 degrees, 90, degrees, and 150 degrees were used to account for each type of bifurcation angle, acute y-Type, T-type, and obtuse y-Type. For simplicity, the dimensional characteristics of the bifurcation model is based on the parent vessel diameter, D , a value of $10\ \mu\text{m}$ (Noren, 1999) (Fig. 2.2).

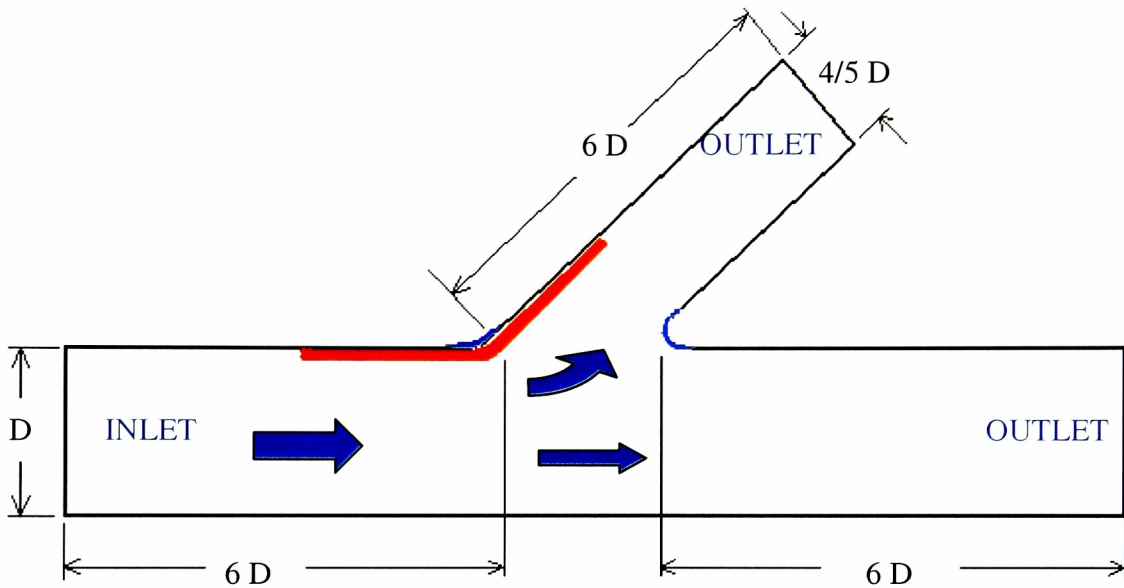


Figure 2.2: Bifurcation Geometry

A diameter ratio of $4/5$ between the branching and parent vessels was maintained for every model. A length of $6D$ for each vessel segment was used in consideration for the typical endothelial cell length of $6D$, nominally distributed equally about the branch corner (Fig. 2.3), developing flow in the entrance and end effects at the flow exit. The developing flow entrance time was determined via comparison of steady-state analysis and transient analysis of blood flow in a straight vessel with the same boundary conditions, outlined later in this chapter, as used in the bifurcation models of interest. Under steady-state conditions, analysis of the flow shows fully developed flow within one vessel diameter length, D , from the inlet. For analysis of the effect of bifurcation

corner geometry on wall shear stress, both the apex (downstream) and branch (upstream) corner radii were varied from sharp angles to a 0.2 D radius for acute angles, and to a 1 D radius for obtuse angles (Fig 2.3).

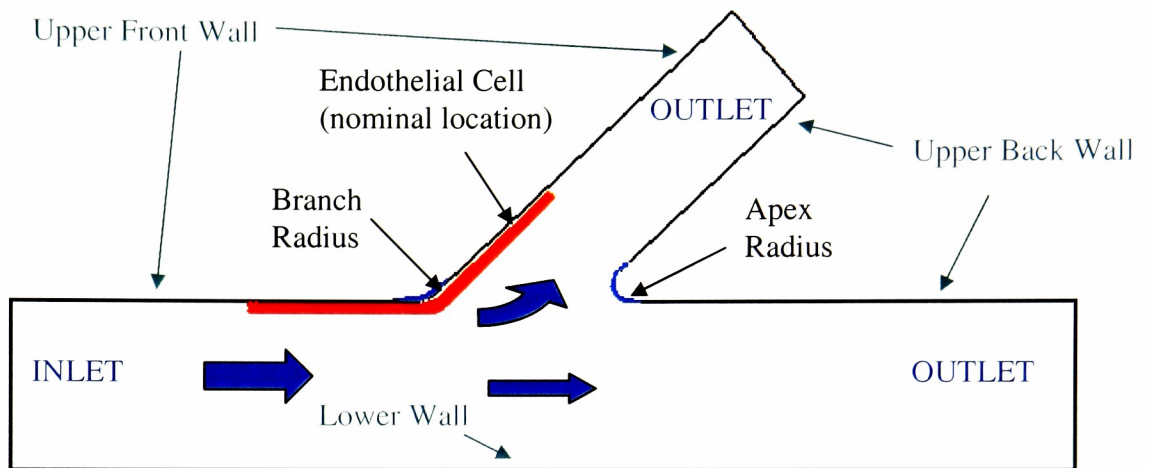


Figure 2.3: Nominal Endothelial Cell Location

Straight channel models were of the shape of rectangles of diameter, D . A length of $8 D$ was chosen to compensate for the same flow end effects as in the bifurcation models and also to provide sufficient length for study of the particle flow behavior during translation through the vessel.

Boundary conditions, which define flow conditions at the edges of the computational geometry, consisted of wall, inlet, and outlet boundaries. Numerical conditions at each of these boundaries remained identical for both the bifurcation and straight channel models. The total velocity on wall boundaries was held constant at zero to instill a realistic, no-slip condition. A uniform, constant, axial velocity was prescribed at the inlet to give a flow Reynolds number of 0.01, which is characteristic of arteriolar flow. Although the outlet boundary was defined as a standard pressure outlet, no

numerical condition was necessary since the flow characteristics at this boundary were to depend entirely on the flow field solution. In the Newtonian studies, the branch to parent vessel flow split was kept constant at 30% to accommodate comparison to Noren (1999). However, for the particulate flow studies, the flow split was not prescribed, but determined during the solution of the conservation equations. Specifically, the pressure drop from model inlet to model outlet was a direct result of the imposed velocity inlet condition (Fluent, 2001).

For the two-dimensional bifurcation and straight channel models, the continuous fluid continuum was decomposed to a discrete grid of quadrilateral elements with an average interval size of $0.3\mu\text{m}$, a nominal 30 elements across the $10\mu\text{m}$ diameter (Fig 2.4). This relative interval size was consistent among all of the two-dimensional and three-dimensional Newtonian flow and particulate flow studies of straight channel and bifurcating geometries.

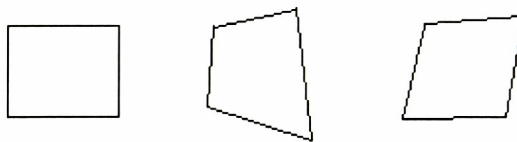


Figure 2.4: Quadrilateral Elements

The element size of $D/30$ was sufficiently small enough to capture important flow detail at the wall boundaries, however large enough to prevent use of an excessive number of elements.

The mesh scheme used for the three-dimensional simulations was slightly different from that used for the two-dimensional analyses. The more complicated three-

dimensional geometry was easily discretized with a tetrahedral meshing scheme. Using this scheme, the compromise of meshing a more complicated model is balanced by a higher number of computational elements. In the three-dimensional studies of this research, the number of elements was not of concern since the geometry of the bifurcating domain was simple. Greater care was taken, however, to appropriately resolve the boundaries of the flow domain.

In consideration for the level of experimental error introduced as a result of the meshing scheme used, the numerical approximation methods developed in the Fluent and FIDAP software programs have introduced corrections to minimize associative calculation errors, namely second order discretization methods (Fluent, 2001).

In order to model the particulate nature of blood, specifically, erythrocyte flow in plasma, the initial location and size of a red blood cell presence within the plasma fluid domain was defined. To accommodate the square element grid of the continuum, the initial RBC shape was chosen to be square, with one side tangent to the model inlet (Fig. 2.5). The size of the initial droplet square was determined to have equivalent two-dimensional area to that of a typical erythrocyte (calculated for a circle of diameter of $5\ \mu\text{m}$). Although the initial shape of the droplet in the domain may be any initial size, due to the discrete nature of the solution process, the square initial shape best accommodates the quadrilateral domain discretization and solution efficiency (lower number of computational elements). The initial droplet size does not, however, have any effect on the solution results, as shown by analysis, in that the defining properties of the droplet fluid and of the surrounding fluid cause the droplet to develop into a circular shape within one vessel diameter length ($10\ \mu\text{m}$).

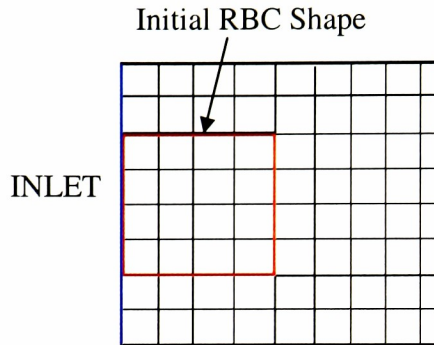


Figure 2.5: Particle Model Definition

2.2

Governing Equations

The continuity equation, momentum equation, and energy equation govern the predicted solution to all possible types of fluid flow. The solution of the continuity and momentum equations are required for the solution of any fluid flow, whereas the energy equations is required when heat energy is present. In this research, heat energy is not a consideration and the solution to the flow relies on the solution of the continuity and momentum equations only.

For a two-dimensional, Eulerian flow field (spatially fixed grid), the differential form of the continuity equation, 2.1, and the momentum equation, 2.2, are given (Fluent, 2001)

$$\frac{\partial \rho}{\partial t} + \frac{\partial u}{\partial x} + \frac{\partial v}{\partial y} = 0 \quad \text{[Equation 2.1]}$$

$$\rho \left(\frac{\partial \mathbf{V}}{\partial t} + u \frac{\partial \mathbf{V}}{\partial x} + v \frac{\partial \mathbf{V}}{\partial y} - \mathbf{g} \right) - \mu \left(\frac{\partial^2 \mathbf{V}}{\partial x^2} + \frac{\partial^2 \mathbf{V}}{\partial y^2} \right) + \nabla p = 0 \quad [\text{Equation 2.2}]$$

where u and v represent the x and y components of the velocity vector, \mathbf{V} , and p , μ , ρ , \mathbf{g} , and t represent pressure, absolute viscosity, density, the gravitational vector, and time, respectively.

2.3

FIDAP Analysis

The software used for the computational analysis was FIDAP 8.6.2, a product of Fluent, Inc. FIDAP applies the governing fluid flow equations, described in section 2.2, via the finite element method to a discrete computational domain. The solution of these equations at each element in the continuum grid is then obtained using numerical techniques and the prescribed initial and boundary conditions.

2.3.1

Volume of Fluid (VOF)

The VOF modeling approach was used to mimic the particle flow behavior exhibited in microcirculation with representation of the RBC presence as a secondary fluid droplet within the primary, plasma fluid. In this approach, fluid density, viscosity, and surface tension are controlling properties that determine droplet flow behavior, shape and translational characteristics (Fluent, 2001).

In FIDAP, the VOF model allows for the solution of transient, free surface flows, the free surface being the interface between two immiscible fluids or a fluid and a gas

(Fluent, 2001). Transient deformations of a free surface may be of arbitrary shape and are predicted by an alternation between a volume tracking method and the finite element method (Fluent, 2001). First, the volume tracking method determines the new fluid boundary based on the given velocity field, then the finite element method is used to predict the fluid kinematics (Fluent, 2001).

In applying the volume of fluid model, all fluid elements within the computational mesh are defined with a volume of fluid type, the interface of which represents the free surface. To do this, FIDAP uses a characteristic marker concentration factor, f_i , which designates the fractional fill state of each element, i , for any time, t (Fluent, 2001). This fill state may vary between 0 and 1 for any element during an analysis (Fluent, 2001). For the two fluid case illustrated in figure 2.6, a fill state of 1 represents fluid A, a fill state of 0 represents fluid B, and a fractional fill state represents the free surface boundary.

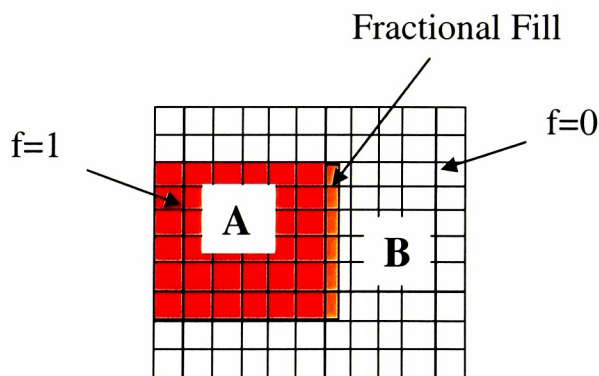


Figure 2.6 Fractional Fill Diagram

In the volume tracking method, the advection of the fluid fill state is governed by equation 2.3, which insures fluid conservation for each element (Fluent, 2001). Recall that an Eulerian description of the flow field is used so the mesh elements remain fixed.

$$\frac{\partial \mathbf{F}}{\partial t} + \mathbf{v} \bullet \nabla \mathbf{F} = 0 \quad \text{[Equation 2.3]}$$

Correspondingly, the fluid kinematics are governed by the finite element formulation of the fluid flow conservation equations, 2.1 and 2.2.

As a counterpart to the Volume of Fluid method, a fluid surface tension definition is introduced to dictate behavior at the interface between the two fluids. Figure 2.7 considers the case of an ideal, spherical droplet where p_o and p_i are the fluid pressures outside and inside the droplet and R is the droplet radius.

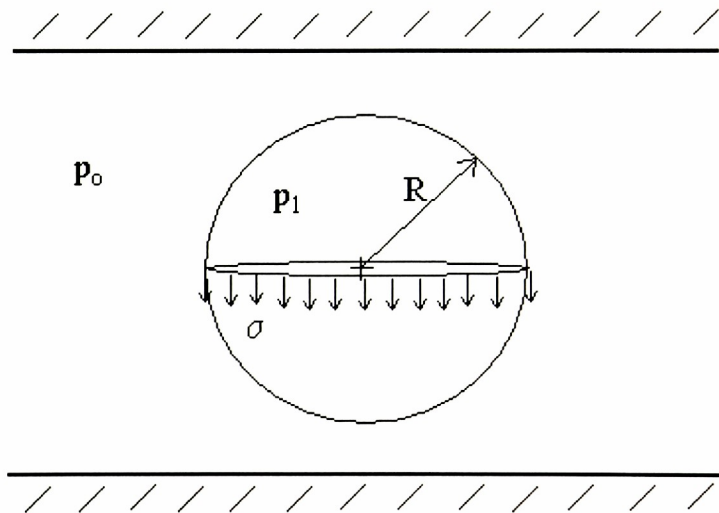


Figure 2.7: Surface Tension of a Spherical Droplet

The surface tension across the two fluid interface causing a normal stress jump, which results in a pressure difference, which preserves the droplet's shape. In FIDAP, this discontinuity is characterized by the following surface traction condition

$$\begin{aligned}\sigma_n^A - \sigma_n^B &= 2\gamma H \\ \sigma_t^A - \sigma_t^B &= 0\end{aligned}\tag{Equation 2.4}$$

where γ is a surface tension coefficient (N/m), H is the mean curvature of the fluid interface surface (1/m), and σ_n and σ_t represent the normal and tangential components of surface stress inside and outside the sphere (Fluent, 2001). Fluid A corresponding to the red blood cell fluid and fluid B corresponding to the plasma fluid.

2.3.2 FIDAP FEM Formulation

The solution of the governing fluid flow equations is not trivial; it involves the use of sophisticated numerical techniques. In FIDAP, the numerical description of the governing fluid flow equations is accomplished by the finite element method.

The finite element formulation replaces the governing partial differential equations with linear interpolation functions, reducing the initial nonlinear continuum problem to a linear discrete problem. This transformation results in a system of algebraic equations for solution rather than solving the governing partial differential equations directly, as in the finite difference method. The formulation of linear algebraic equations makes the finite element method ideal for problems of complicated geometry.

Several methods exist for formulation of the discrete problem. In all cases, the stiffness matrix and algebraic equations are defined for each element and are easily expressed in matrix notation, in the form $[F] = [F]_{n \times m}$. The element nodal equations are then combined to form the global stiffness equation, of the form $[F] = [k][d]$, where $[F]$ represents the body force matrix, $[k]$ represents the global stiffness matrix, and $[d]$ represents the nodal displacement matrix.

As mentioned, the solution of these equations is far from trivial, and may require some numerical stability on convergence to a solution. For this, FIDAP takes advantage of an advanced numerical method, applicable to the finite element method, the Galerkin Weighted Residual method. FIDAP then solves the governing fluid flow equations, defined in section 2.2, given the boundary and continuum definitions, at each of the nodes in the fluid domain under the control of the solver setting parameters.

With the application of the Galerkin finite-element method, the complete formulation of the governing equations for an unsteady, incompressible flow of two immiscible fluids, with negligible gravitational effects becomes (Fluent, 2001)

$$\int_V \left(\frac{\partial \mathbf{V}}{\partial t} + \nabla \cdot \mathbf{V} \right) \psi_k dV = 0 \quad \text{[Equation 2.4]}$$

$$\int_V \rho \left(\frac{\partial \mathbf{V}}{\partial t} + \mathbf{V} \cdot \nabla \mathbf{V} \right) \phi_i dV + \int_V (\nabla \tau - p \mathbf{I}) \cdot \nabla \phi_i dV = \int_A \boldsymbol{\sigma} \cdot \mathbf{n} d\phi_i dA \quad \text{[Equation 2.5]}$$

The last term of the momentum equation, $\boldsymbol{\sigma} \cdot \mathbf{n}$, represents the surface traction

condition, which results from the presence of surface tension at the two fluid interface, S (Fluent, 2001). The stress balance across the two fluid interface is given by 2.6 (Fluent, 2001).

$$\left(\mathbf{T} \cdot \mathbf{n} - \hat{\mathbf{T}} \cdot \mathbf{n} \right) \cdot \mathbf{n} = \sigma (\nabla_s \cdot \mathbf{n}) \quad \text{[Equation 2.6]}$$

where \mathbf{T} and $\hat{\mathbf{T}}$ are the stress tensors for both fluids, \mathbf{n} is the normal to the fluid interface surface, σ is interfacial tension, and ∇_s is the surface gradient operator (Fluent, 2001).

For a spherical interface, S , we have equation 2.7

$$\nabla_s \cdot \mathbf{n} = \left(\frac{2}{R} \right) \quad \text{[Equation 2.7]}$$

where R is the spherical radius. Note that the left side of the first equation in 2.4 is consistent with equation 2.6.

2.4 Analysis Concerns

Several issues arose in the development of the computational arteriole models. In consideration for accurate, however efficient results of the flow behavior, the material properties of the red blood cell and plasma and the resolution and skewness of the continuum grid become particularly important.

The development of the continuum grid was governed by the importance of understanding flow properties along the vessel walls. Furthermore, the grid size throughout the entire flow domain determined the resolution of the droplet interface with the surrounding plasma. As a result, an interval size of $0.3\mu\text{m}$ was chosen so as to give sufficient resolution near the wall boundaries and throughout the flow domain while compromising with the cost of computational availability and efficiency.

Another concern involved the quantified effect of surface tension on the flow properties near the vessel wall, if any. Since RBC's aren't characterized with surface tension properties, the corresponding surface tension value used in analysis was to be experimentally determined, based on comparisons of flow behavior and effect on flow properties.

Chapter 3

Wall Shear Stress Analysis

Understanding flow characteristics as sensed by the endothelial cell lining in arteriolar vessels is a major component of comprehending microcirculation. This research is dedicated to introducing a substantial simplification to the computational modeling approach and to depicting, in greater detail, the relationship of corner geometry and the presence of RBCs to flow behavior as sensed by the endothelial cells.

3.1

Computational Validation

The first phase of this research involved the duplication of previously predicted three-dimensional computational results. This included a comparison of two-dimensional and three dimensional wall shear stress characterizations to certify a two-dimensional modeling simplification as an accurate method of prediction. An apparent viscosity of blood was used to simulate equivalent whole blood flow behavior through an arteriole bifurcation. An apparent viscosity value for whole blood of Golden Hamsters, 0.001 Ns/m^2 , characteristic flow split of 30% to the branch, and characteristic flow Reynolds number of 0.01 was used (Frame and Sarelius, 1996).

3.1.1

Comparison of Two-Dimensional Results to Three-Dimensional Results

Typically, three-dimensional flow problems are described with a three-dimensional computational fluid domain. This research suggests, for simplification, the use of a two-

dimensional computational model. To show accuracy of prediction capability, a comparison of normalized results from a two-dimensional analysis and three dimensional analysis results was made using equivalent bifurcation geometry with blood modeled as a Newtonian fluid as before.

Figures 3.1, 3.2, and 3.3 show the comparison results for 30 degrees, 90 degrees, and 150 degrees, respectively, along the parent wall for case studies of this research. The results of the two-dimensional studies effectively represent the geometry of the mid-plane of the three-dimensional model. Wall Shear stress values shown in each of these three figures, relative to the average value at any wall position, shows a consistent variation of thirteen percent in shear values axially along the parent branch of the bifurcation. The wall shear stress shown is a total wall shear stress determined from $\tau_w = \frac{\partial V}{\partial n}$, which reflects velocities in the three coordinate directions, x, y, and z and is calculated using a localized normal to the boundary that is independent of orientation relative to the coordinate axis. The variation in wall shear stress observed in the three dimensional studies is caused by an insufficiently resolved boundary layer, according to Equation 3.1, developed from the Blasius solution for laminar flow over a flat plate (Fluent 2001).

$$y_p \sqrt{\frac{u_\infty}{\nu x}} \leq 1 \quad [\text{Equation 3.1}]$$

In this equation, y_p is the distance of the adjacent cell centroid from the wall, u_∞ is the freestream velocity, ν is the kinematic fluid viscosity, and x is the distance along the wall from where the boundary layer begins (Fluent 2001).

The calculated value of y_p nearer the flow inlet of the flow model of 0.067 is smaller than the nominal centroid size near 0.15 actually used in discretizing the flow

domain, which suggests that the mesh need to be revised using a nominal element size of 0.13, satisfying the relationship given by Equation 3.1.

In a comparison of normalized values, the general trend of shear stress behavior in the three dimensional analysis was captured agreeably by the two dimensional analysis. Values predicted by the simplified analysis fall into the lower region of the range of values given by the three-dimensional model results (Figures 3.1-3.3). Furthermore, the wall shear stress variation shown in the three-dimensional results is consistent, which gives itself to numerical prediction from the two-dimensional model values.

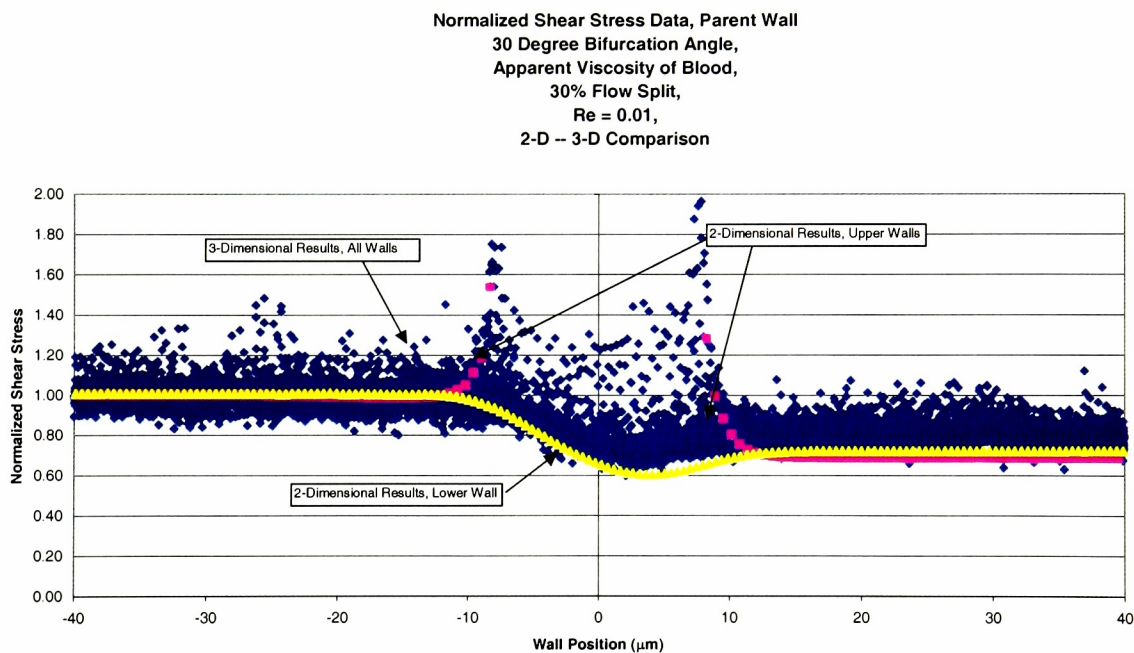


Figure 3.1: 2D-3D Wall Shear Stress Comparison, 30 degree Bifurcation

Shear Stress Data, Parent Wall
90 Degree Bifurcation Angle,
Apparent Viscosity of Blood,
30% Flow Split,
Re = 0.01,
2-D -- 3-D Comparison

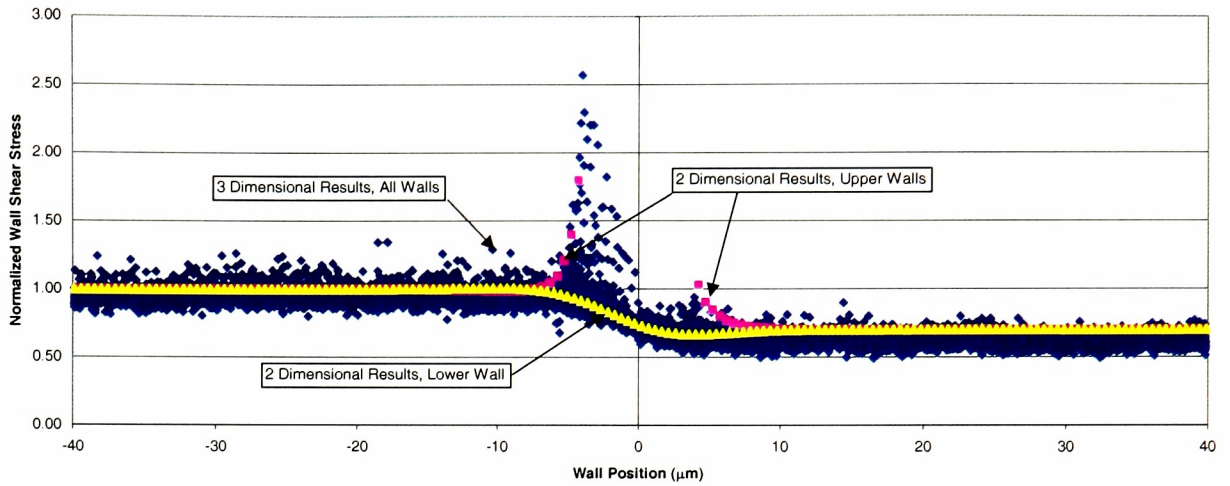


Figure 3.2: 2D-3D Wall Shear Stress Comparison, 90 degree Bifurcation

Shear Stress Data, Parent Wall
150 Degree Bifurcation Angle,
Apparent Viscosity of Blood,
30% Flow Split,
Re = 0.01,
2-D -- 3-D Comparison

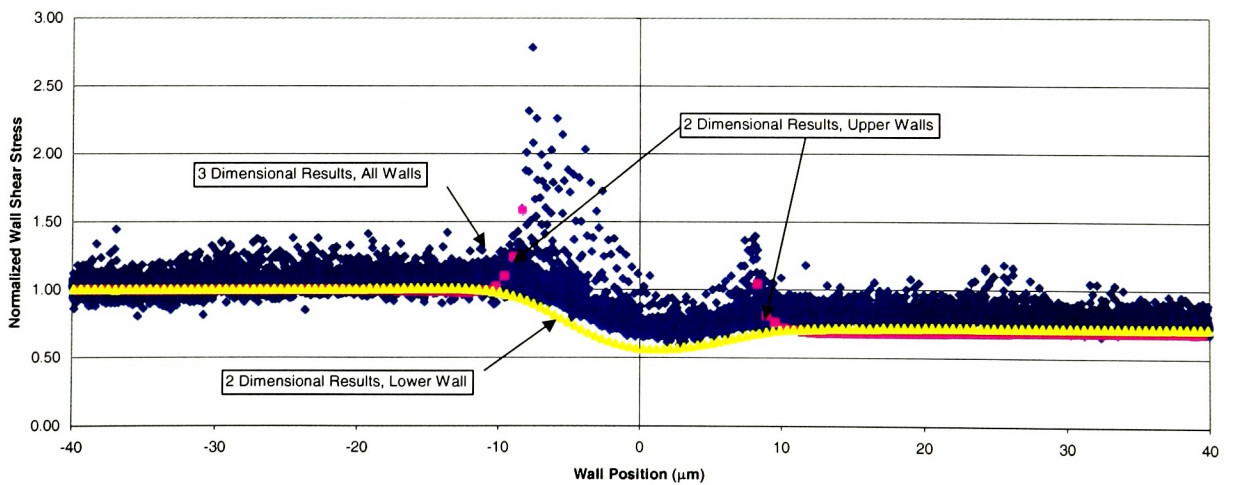


Figure 3.3: 2D-3D Wall Shear Stress Comparison, 150 degree Bifurcation

3.1.2

3.1.2

Wall Shear Stress Comparisons to Published Studies in Golden Hamsters

Predicted *in vivo* three-dimensional wall shear stress gradients in arteriolar bifurcations of the Hamster cremaster muscle and predicted computational values (Noren, 1999) were duplicated by three-dimensional analyses in this research. The agreeable comparison not only verified computational ability, but also acknowledged integrity in the solution methodology. The shear stress values were normalized to a constant upstream value to accommodate numerical comparison. Figures 3.4, 3.5, and 3.6 show the comparison results of the two-dimensional model from the current study with the three-dimensional simulation results and *in vivo* data (Noren, 1999) for the 30 degree, 90 degree, and 150 degree bifurcations, respectively.

The two-dimensional prediction of this investigation shared a common curve shape with the (Noren, 1999) values for 30, 90, and 150 degree bifurcations, however, in much greater detail with data at nearly 100 discrete points as opposed to four. Noren (1999) predicted wall shear stress was estimated from transverse velocity profiles at four discrete locations, one upstream of and downstream of the junction where the velocity profile was parabolic (undisturbed by the flow disturbance of the junction), at the apex corner, and at the branch corner (Noren, 1999). In areas of the greatest flow perturbation, on either side of the bifurcating branch, the upper wall predictions made in this study were nearly two times lower than the computational predictions made in Noren (1999). However, the values presented by this research compared well with the *in vivo* results presented for comparison in Noren (1999) (Figures 3.4-3.6). The discrepancy between the results shown in this research and those presented in Noren (1999) may be attributed

to the linear approximation technique used in Noren (1999), where wall shear stress was calculated from numerical values of a transverse velocity profile.

Noren (1999) values far from the bifurcation, where flow is most laminar, compared well with the two-dimensional results from the present study. Wall shear values upstream of the bifurcation, used for normalization, were equivalent. The wall shear stress values predicted downstream of the bifurcation were nearly 0.25 times larger than those *in vivo* (Noren, 1999) and equivalent to those predicted (Noren, 1999). The variance of the *in vivo* wall shear stress values downstream of the bifurcation could be due to the visual observation of the slightly increasing feed branch vessel diameter in the same direction of blood flow, which lowers flow velocity and therefore, wall shear stress.

Normalized Shear Stress Data, Parent Wall
 30 Degree Bifurcation Angle,
 Apparent Viscosity of Blood,
 30% Flow Split,
 $Re = 0.01$

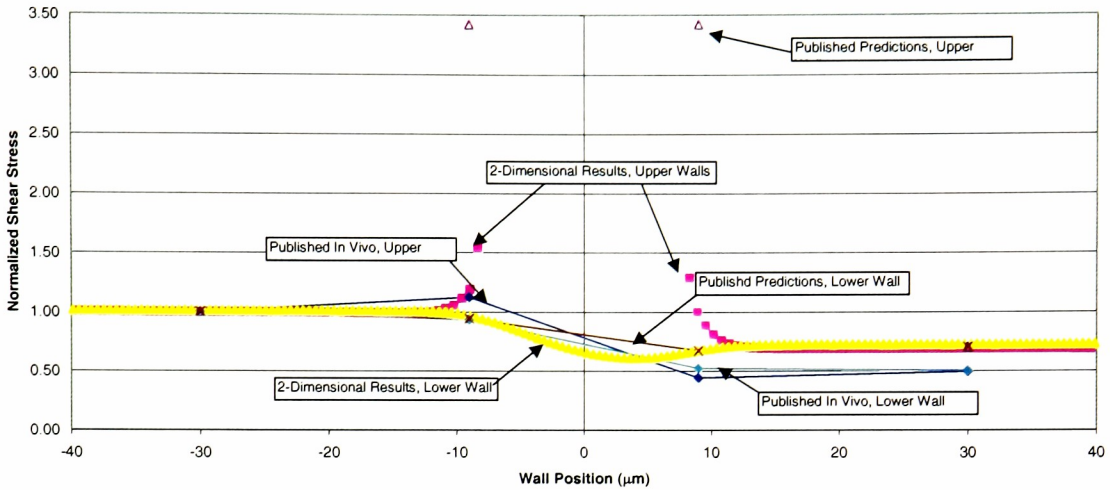


Figure 3.4: 2-D Comparison to In Vivo and 3D Simulation Data (Noren, 1999),
 30 Degree Bifurcation

Shear Stress Data, Parent Wall
 90 Degree Bifurcation Angle,
 Apparent Viscosity of Blood,
 30% Flow Split,
 $Re = 0.01$

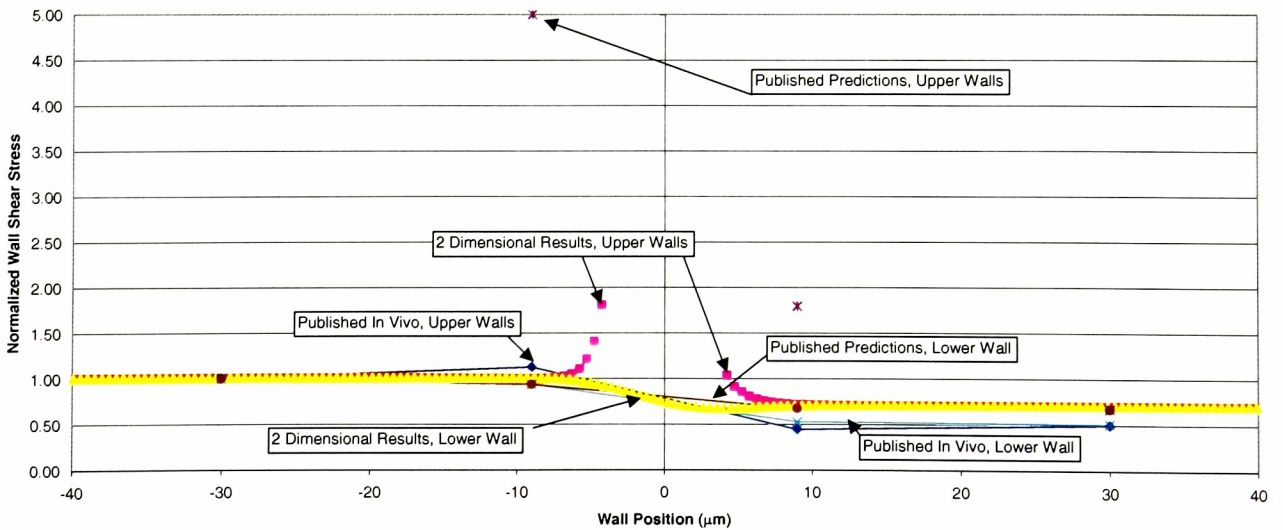


Figure 3.5: 2-D Comparison to In Vivo and 3D Simulation Data (Noren, 1999),
 90 Degree Bifurcation

Shear Stress Data, Parent Wall
150 Degree Bifurcation Angle,
Apparent Viscosity of Blood,
30% Flow Split,
 $Re = 0.01$

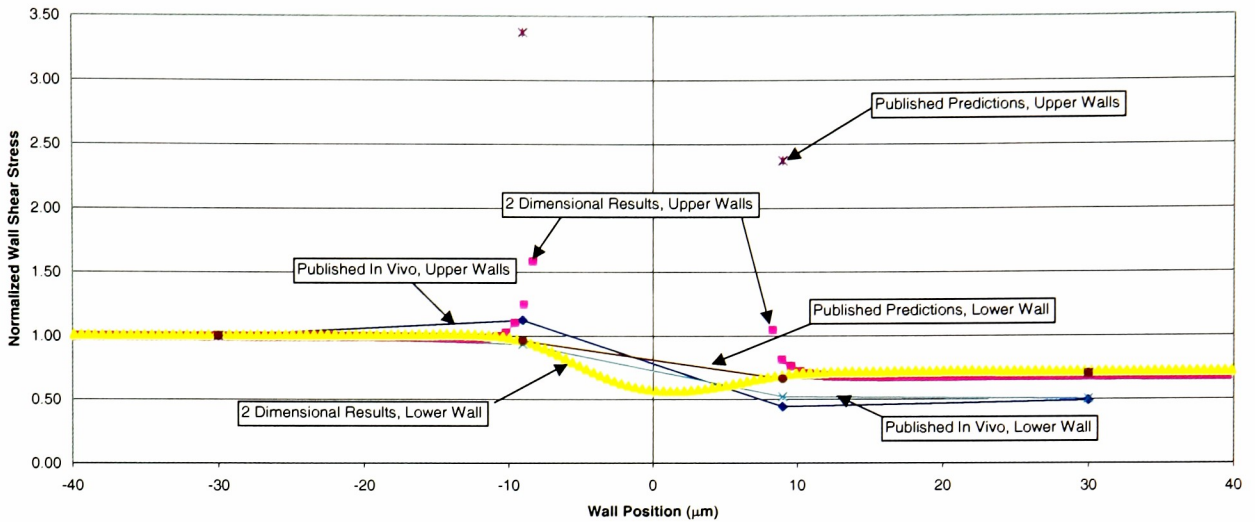


Figure 3.6: 2-D Comparison to In Vivo and 3D Simulation Data (Noren, 1999),
150 Degree Bifurcation

3.2 Influence of Corner Geometry

After qualification of the simplified modeling approach and agreement of wall shear predictions in regular, sharp-corner geometry, the arteriolar bifurcating blood flow investigation carried forward to the variation of wall shear stress as a direct result of the model geometry at the apex and branch locations. The corner geometry of each bifurcation was changed systematically to determine the specific influence of each change on wall shear stress. The geometry of all acute exterior angles were varied from sharp to a radius of $1\mu\text{m}$ and $2\mu\text{m}$. In a similar manner, the geometry of all exterior obtuse angles were varied from sharp to a radius $5\mu\text{m}$ and $10\mu\text{m}$. The approximation of

blood behavior as Newtonian was maintained again in this study of 30, 90, and 150 degree bifurcations for standard comparison. For each bifurcation geometry, wall shear stress was normalized to a constant upstream value to accommodate comparison. Characterizations of these values axially along the upper front, upper back, and lower bifurcation walls, are plotted against baseline values established by analysis of the regular geometry with sharp corners.

All results reveal a characteristic reverse “s” shape in wall shear stress with a local maximum and local minimum shear stress value as shown in Figure 3.7.

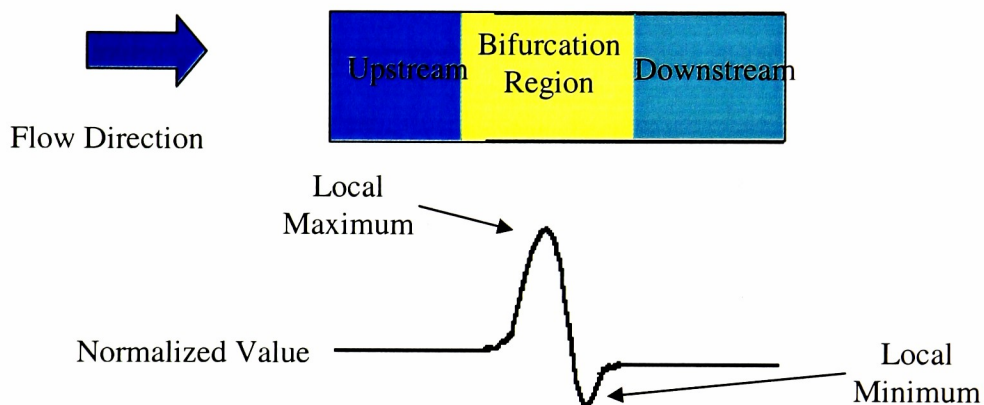


Figure 3.7: Characteristic “s” Shape in Bifurcation Wall Shear Stress

The drop in wall shear stress, the minimum, corresponds with the change in bifurcation area. As the area increases, as a result of changing corner geometry, the wall shear stress minimum is shown to decrease, and in some cases shift. Further information regarding the bifurcation size for each model geometry considered in the corner geometry influence on wall shear stress is provided in section A1 in the appendix.

Included with the graphical results for each study is a gradient, or temporal average of the shear stress values. The values are averaged bi-directionally at an axial

range of three main branch diameters, thereby representing the stimuli on a sensing surface of a typical endothelial cell lining the vessel wall.

For each scenario presented in this section, the value of normalized wall shear stress can be approximated in each extremity of the bifurcation using the corresponding flowrate and diameter. In all cases a 30% flow split, to the branch, was defined. Since wall shear stress is proportional to velocity and since flowrate is proportional to velocity, a drop in normalized wall shear stress given constant diameter is predictable from the corresponding drop in flow rate. For the inlet to parent bifurcation segments, the normalized wall shear stress shown in the following graphs drops from 1.0 to nearly 0.7, corresponding with the drop in flowrate of 30%, since the respective diameters of each bifurcation segment are equivalent. For the 70% drop in flowrate from the inlet to branch segment, the normalized wall shear stress shown for the branch vessel is nearly 0.5, 20% higher than an expected value of 0.3, given equivalent vessel diameters. The increase observed in normalized wall shear stress of the branch segment counters the 20% decrease in the branch diameter compared to the parent diameter.

Upper Front Wall

Figures 3.8-3.10 show normalized wall shear stress characterizations along the upper front wall within the region where a typical endothelial cell would line the vessel wall, as explained in Chapter 2. Specifically, Figures 3.8a and 3.8b show wall shear stress for 30 degree bifurcations with varying corner radii with a constant branch radius of 10 μ m and constant apex radius of 1 μ m, respectively. Figure 3.9 shows wall shear stress with varying corner radii which is symmetric horizontally. In similar manner to Figures 3.8a and 3.8 b, Figures 3.10a and 3.10b show wall shear stress for a 150 degree

bifurcation with varying corner radii with a constant branch radius of $10\mu\text{m}$ and constant apex radius of $1\mu\text{m}$, respectively. In both the 30 and 90 degree bifurcations, maximum wall shear stress in the parent vessel is lowered by as much as 33% as a result of increasing the branch radius. In the 150 degree bifurcation model, however, an opposite effect is observed. The presence of the radius hinders flow separation at the wall, increasing the wall shear stress. The apex radius had an equally significant effect on the wall characteristics as well. The local wall shear stress minimum was lowered by 29% in the 30 degree bifurcation and increased by 15% in the 150 degree bifurcation.

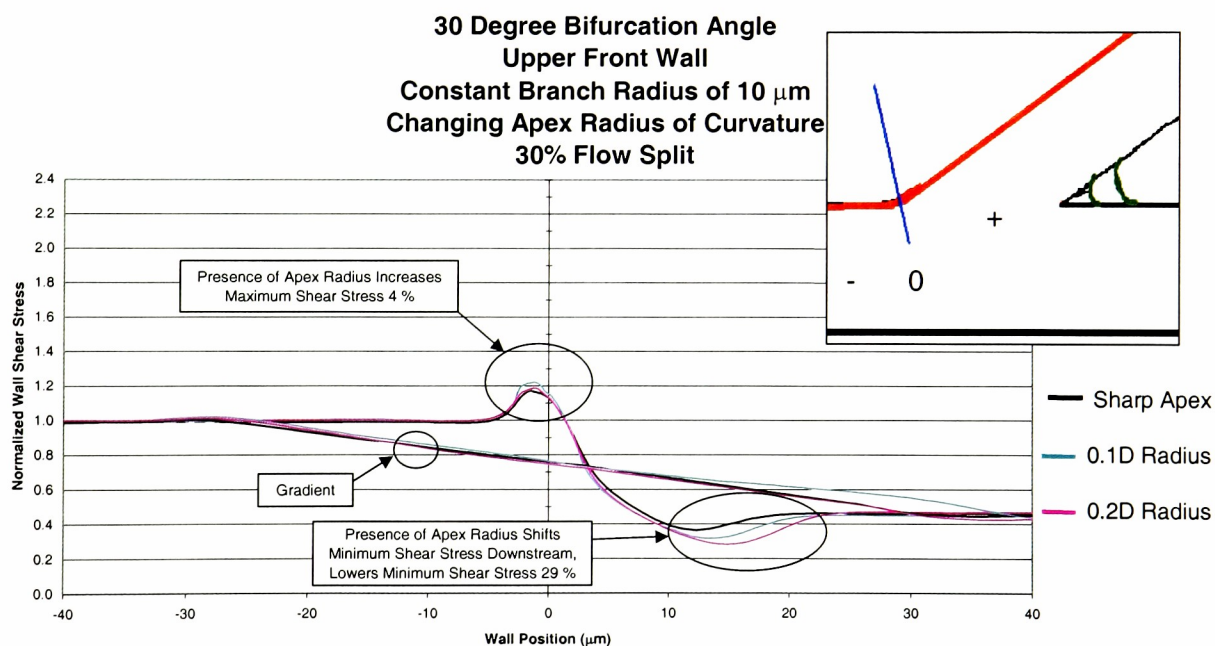


Figure 3.8a: Upper Front Wall Shear Stress, 30 degree Bifurcation

30 Degree Bifurcation Angle
Upper Front Wall
Constant Apex Radius of 1 μm
Changing Branch Radius of Curvature
30% Flow Split

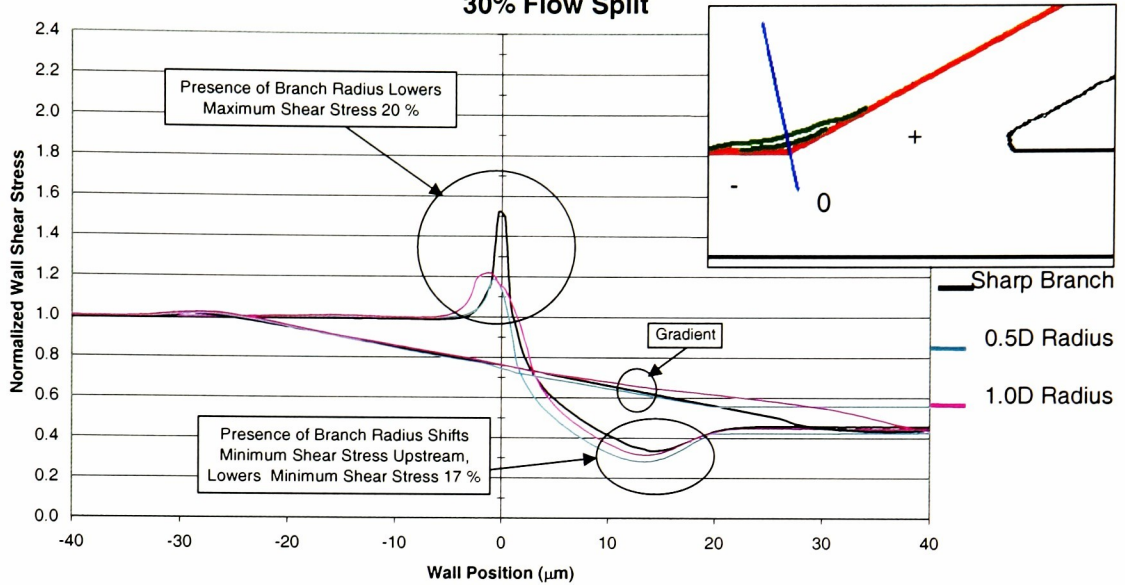


Figure 3.8b: Upper Front Wall Shear Stress, 30 degree Bifurcation

90 Degree Bifurcation Angle
Upper Front Wall
30% Flow Split

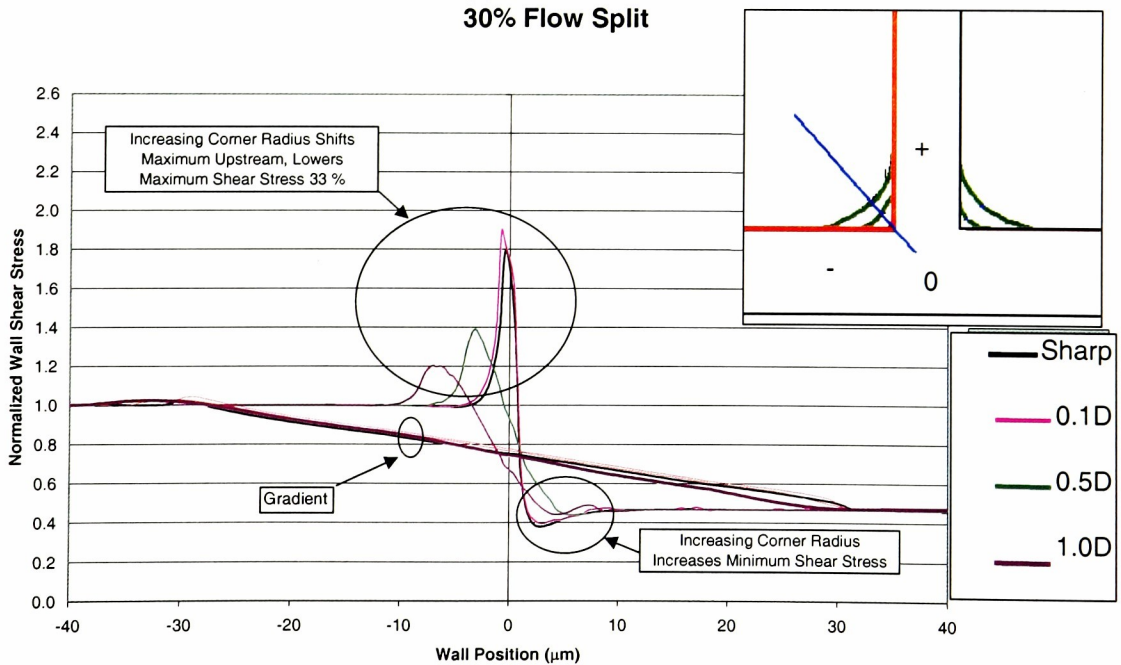


Figure 3.9: Upper Front Wall Shear Stress, 90 degree Bifurcation

150 Degree Bifurcation Angle
Upper Front Wall
Constant Branch Radius of 1 μm
Changing Apex Radius of Curvature
30% Flow Split

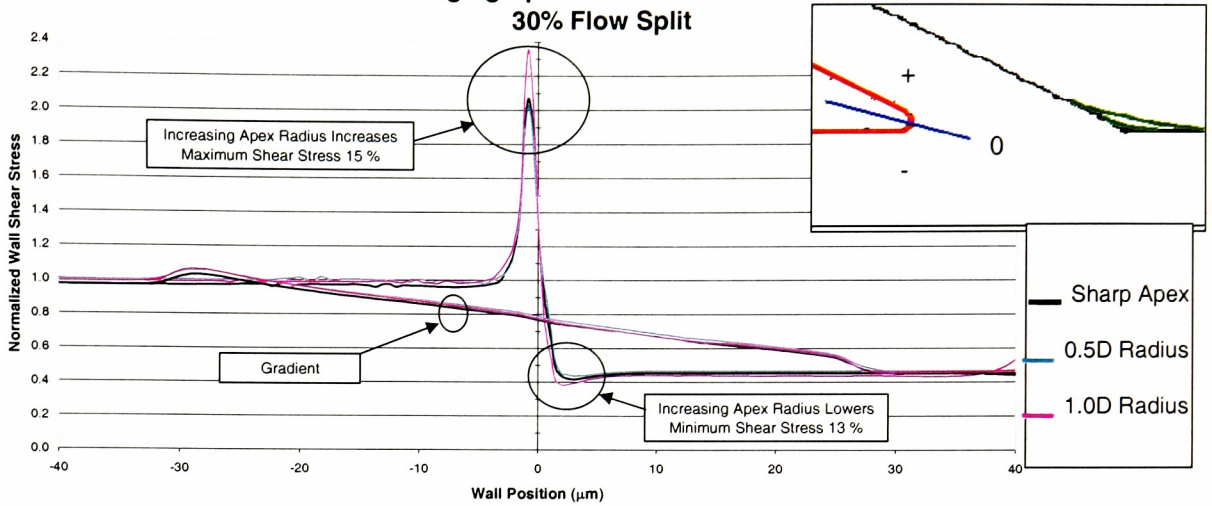


Figure 3.10a: Upper Front Wall Shear Stress, 150 degree Bifurcation

150 Degree Bifurcation Angle
Upper Front Wall
Constant Apex Radius of 10 μm
Changing Branch Radius of Curvature
30% Flow Split

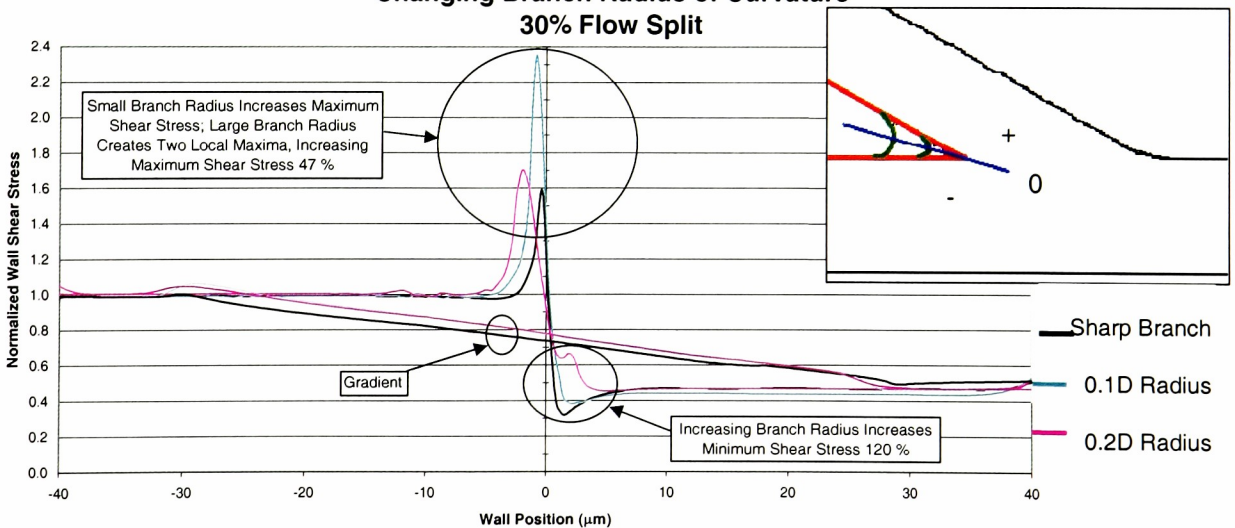


Figure 3.10b: Upper Front Wall Shear Stress, 150 degree Bifurcation

Upper Back Wall

The signature of wall shear stress along the upper back wall of the bifurcating vessel as a result of varying corner curvature is shown in Figures 3.11-3.13. Again, Figures 3.11a and 3.11b show wall shear stress for 30 degree bifurcations with varying corner radii with a constant branch radius of $10\mu\text{m}$ and constant apex radius of $1\mu\text{m}$, respectively. Figure 3.12 shows wall shear stress with varying corner radii which is symmetric horizontally. Figures 3.13a and 3.13b show wall shear stress with varying corner radii with a constant branch radius of $10\mu\text{m}$ and constant apex radius of $1\mu\text{m}$, respectively. For the 90 degree and 150 degree bifurcations, an increase in the apex corner radius was shown to lower the local maximum wall shear stress value in the parent vessel by as much as 90%. The local maximum value of the 30 degree bifurcation model, however, was increased by 33%. The effect of the branch radius in these studies is shown to have only a small effect on the wall shear stress results. In the 30 degree bifurcation, the local maximum in wall shear stress increased by 33% with a $1\mu\text{m}$ radius. In the 150 degree bifurcation, the presence of a $1\mu\text{m}$ radius increases the local maximum by 13%. The local minimum values were lowered by as much as 90% (90 degree bifurcation) and 40% (30 degree bifurcation) with increasing apex radius.

**30 Degree Bifurcation Angle
Upper Back Wall
Constant Branch Radius of 10 μm
Changing Apex Radius of Curvature
30% Flow Split**

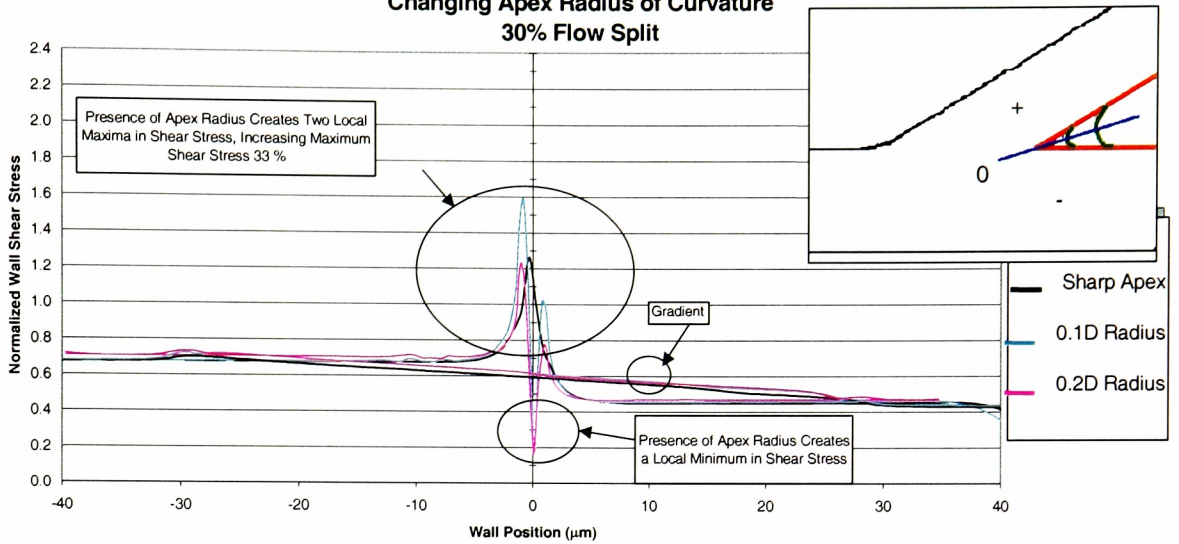


Figure 3.11a: Upper Back Wall Shear Stress, 30 degree Bifurcation

**30 Degree Bifurcation Angle
Upper Back Wall
Constant Apex Radius of 1 μm
Changing Branch Radius of Curvature
30% Flow Split**

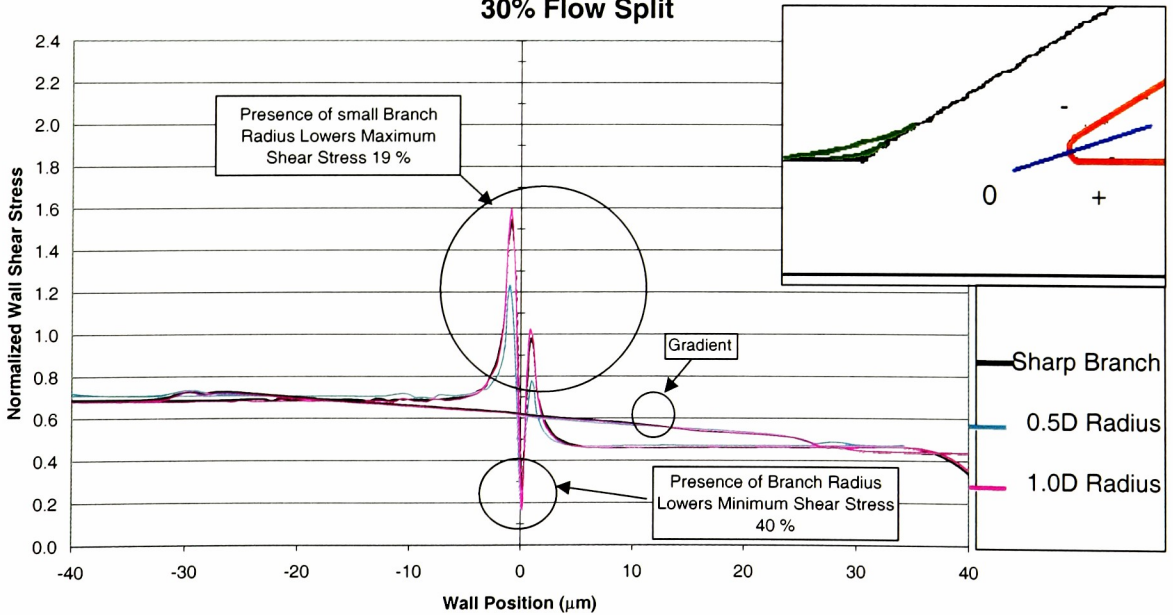


Figure 3.11b: Upper Back Wall Shear Stress, 30 degree Bifurcation

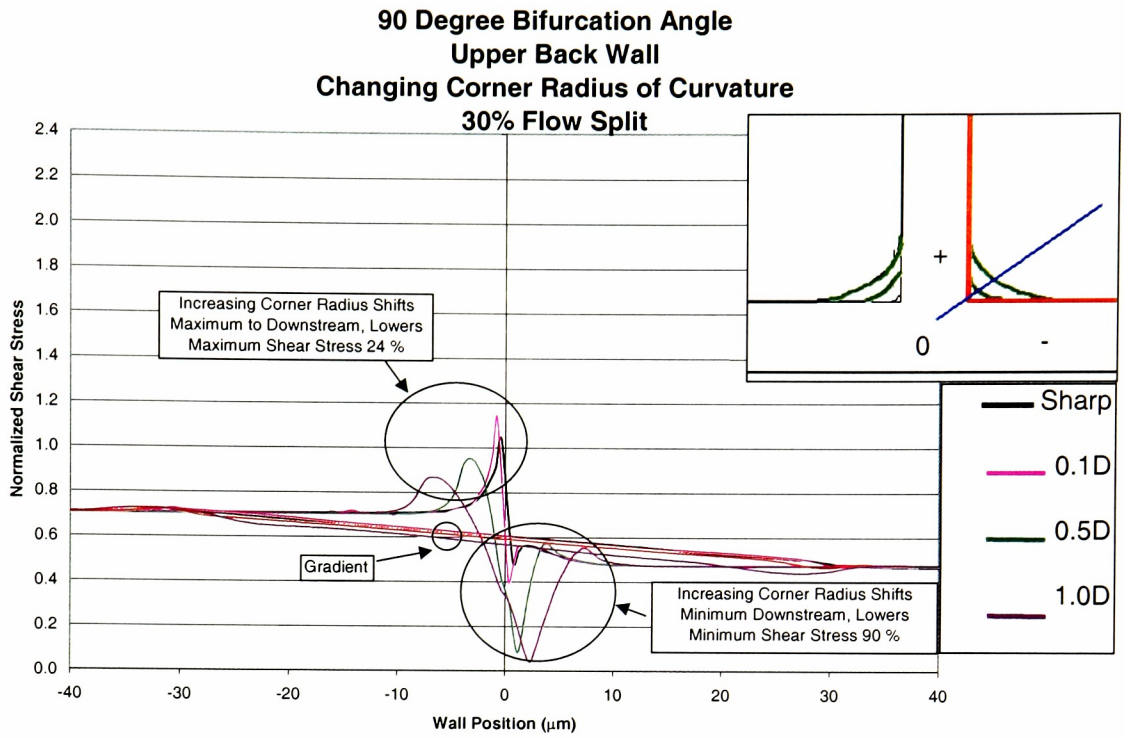


Figure 3.12: Upper Back Wall Shear Stress, 90 degree Bifurcation

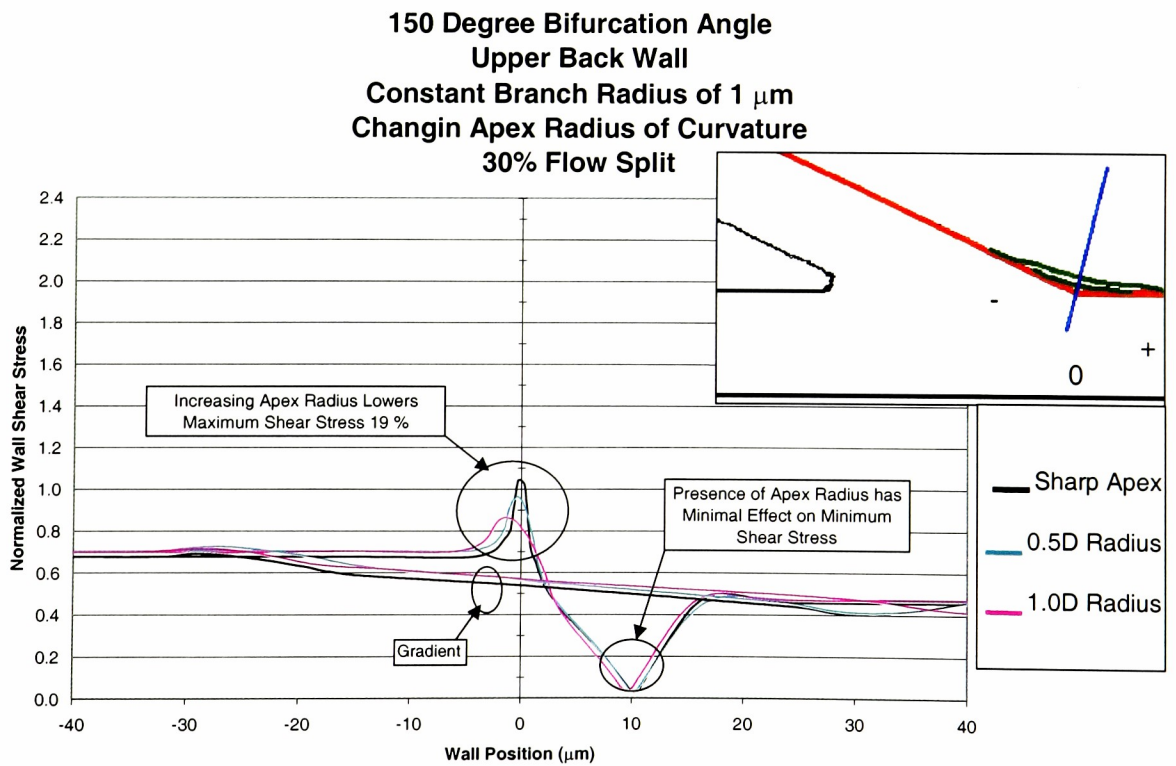


Figure 3.13a: Upper Back Wall Shear Stress, 150 degree Bifurcation

150 Degree Bifurcation Angle
Upper Back Wall
Constant Apex Radius of 10 μm
Changing Branch Radius of Curvature
30% Flow Split

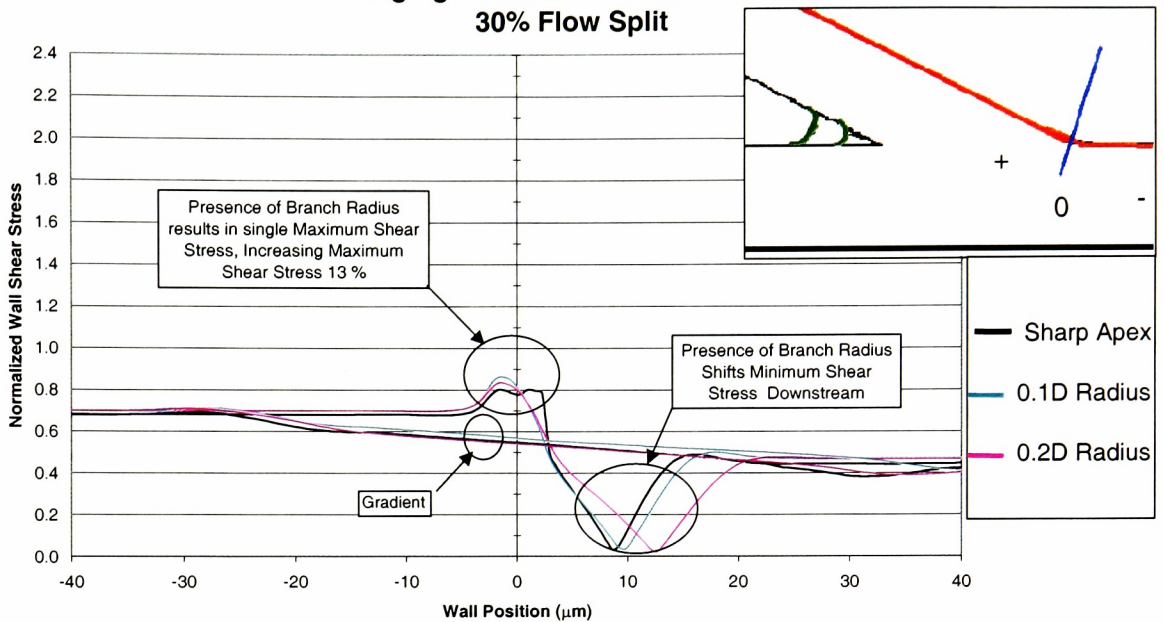


Figure 3.13b: Upper Back Wall Shear Stress, 150 degree Bifurcation

Lower Wall

The wall shear stress characterization along the lower walls of the bifurcation models also shows significant change in wall shear stress as a result of changing corner geometry (Figures 3.14-3.16). Figures 3.14a and 3.14b show wall shear stress for 30 degree bifurcations with varying corner radii with a constant branch radius of $10\mu\text{m}$ and constant apex radius of $1\mu\text{m}$, respectively. Figure 3.15 shows wall shear stress with varying corner radii, which is symmetric horizontally. Figures 3.16a and 3.16b show wall shear stress with varying corner radii with a constant branch radius of $10\mu\text{m}$ and constant apex radius of $1\mu\text{m}$, respectively. The largest influence was caused by an increase in the radius at the acute junctions of the bifurcation. The minimum wall shear

stress was lowered by 25% in the 30 degree bifurcation model, 36% in the 90 degree bifurcation model, and 27% in the 150 degree bifurcation model. Change in the radius at obtuse junctions of the bifurcation model were shown to have only a small influence on the wall shear stress curve.

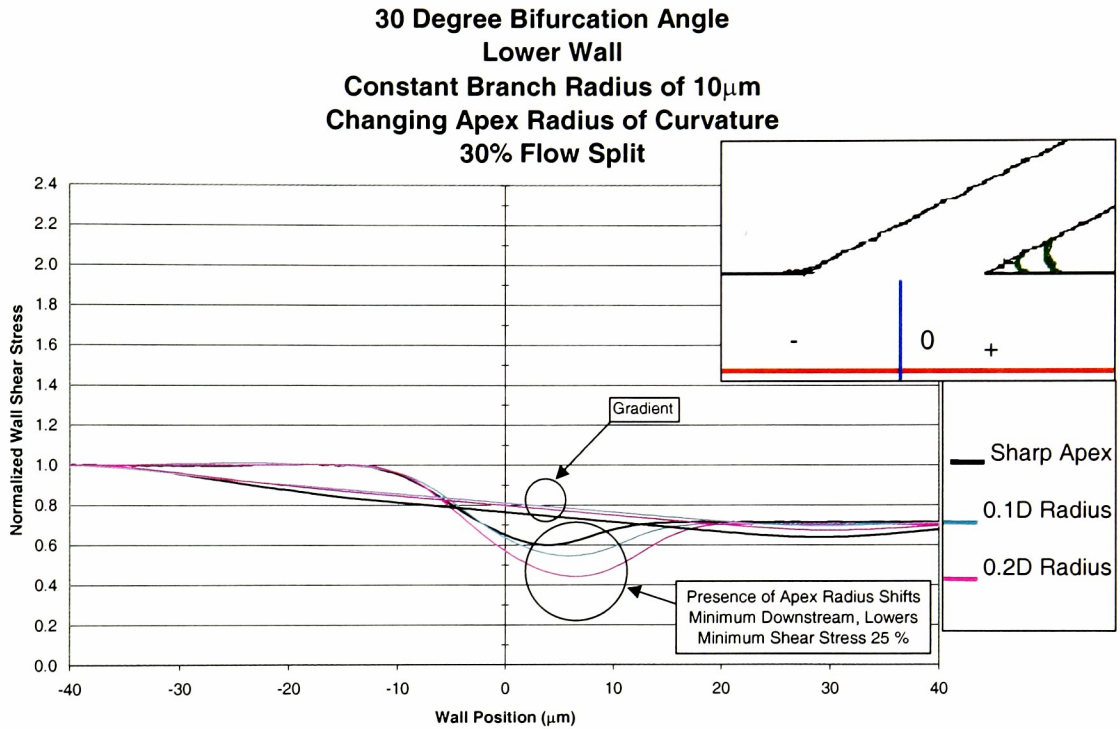


Figure 3.14a: Lower Wall Shear Stress, 30 degree Bifurcation

30 Degree Bifurcation Angle
Lower Wall
Constant Acute Radius of 1 μ m
Changing Branch Radius of Curvature
30% Flow Split

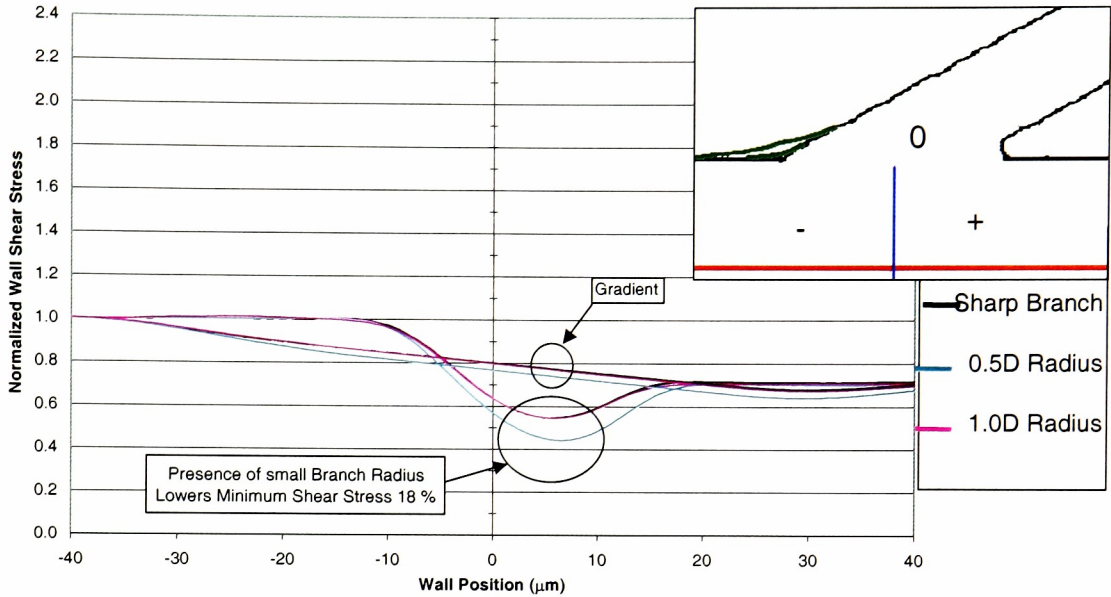


Figure 3.14b: Lower Wall Shear Stress, 30 degree Bifurcation

90 Degree Bifurcation Angle
Lower Wall
30% Flow Split

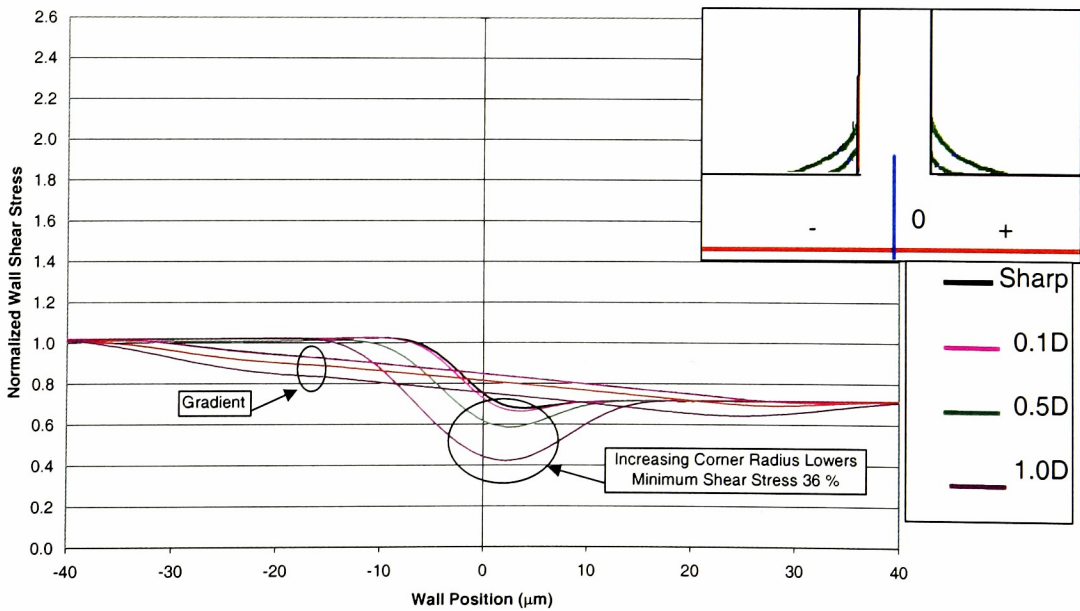


Figure 3.15: Lower Wall Shear Stress, 90 degree Bifurcation

**150 Degree Bifurcation Angle
Lower Wall
Constant Branch Radius of 1 μm
Changing Apex Radius of Curvature
30% Flow Split**

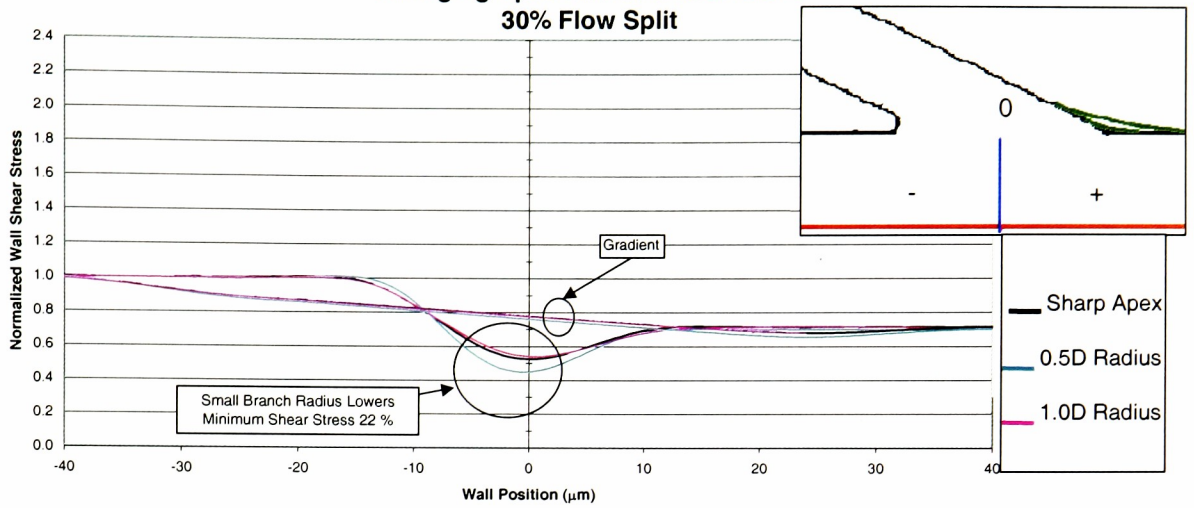


Figure 3.16a: Lower Wall Shear Stress, 150 degree Bifurcation

**150 Degree Bifurcation Angle
Lower Wall
Constant Apex Radius of 10 μm
Changing Branch Radius of Curvature
30% Flow Split**

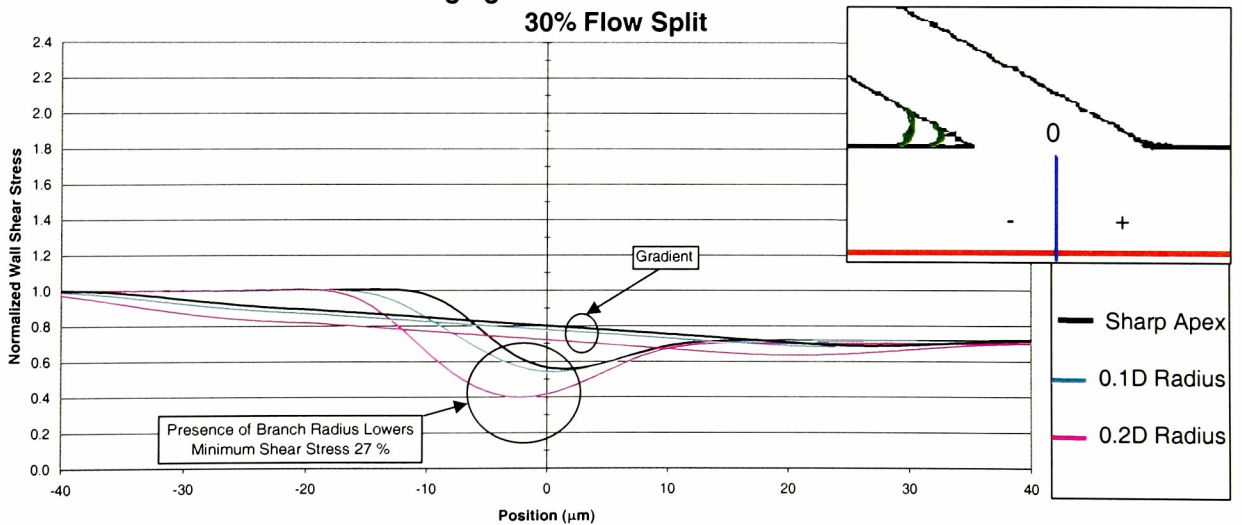


Figure 3.16b: Lower Wall Shear Stress, 150 degree Bifurcation

The Newtonian flow analysis study of varying bifurcation corner geometry shows, with greater detail, a characteristic wall shear stress pattern throughout the bifurcation.

Additionally, these results show changing corner geometry, effectively branch size, does effect wall shear stress. Furthermore, the effect of varying corner geometry on the characteristic wall shear stress pattern changes the local maximum and local minimum values and also shifts the location of each on the wall. As the degree to which changes in wall shear stress pattern effect the responses of the adjacent endothelial cell lining the vessel wall becomes known, accurate computational modeling of the flow may need to account for arteriolar bifurcation corner geometry by default, based on the predictions of this research. In this study, the shear gradient, as determined from the spatial average, is shifted in magnitude as a result of varying corner geometry. Changes in the gradient are minimal as a result of the dissipation of the shear maxima and minima by the relatively large nominal length of $6D$, used to average the wall shear stress.

3.3 Red Blood Cell Presence

The next, most involved area of this study of microcirculatory flow behavior involved the analysis of arteriolar blood flow with the consideration of RBC presence. Considering the actual composition of blood as a fluid laden with red blood cells rather than a Hematocrit based Newtonian fluid was the primary focus. The investigations presented in this segment document the analyses leading up to a refined approach of approximating two-phase blood flow, which includes both straight tube analysis and bifurcation analysis. As before, all wall shear stress characterizations were normalized to a constant upstream value for comparison purposes.

3.3.1 Droplet Presence in a Straight Vessel

For simplicity, flow in a straight vessel was examined first to test the modeling technique of a droplet in a flow and the preliminary effect of the defining viscosity and surface tension values on droplet shape translation (Figure 3.17). These results were later used to define droplet properties in a 30 degree bifurcating flow analysis, where similar translation velocity was observed. These results, however, are discussed in the next section.

Analysis of a droplet-laden flow reveals a localized s-curve wall shear stress pattern (Figure 3.17). The local minimum wall shear stress adjacent to the droplet position suggests a small velocity gradient characteristic of a flat transverse velocity profile. The local maximum value just upstream of the droplet position indicates a larger velocity gradient, characteristic of a velocity profile of higher amplitude.

In the 30 degree bifurcation analysis, however, the shape of the droplet in the region of the bifurcation apex was distorted. Since the only control over droplet behavior lies with the fluid property values, the distortion observed from analysis suggested changing these values, namely fluid surface tension and droplet viscosity. This was accomplished with an evaluation of the several different property values and the corresponding observation of flow behavior in the region of the bifurcation.

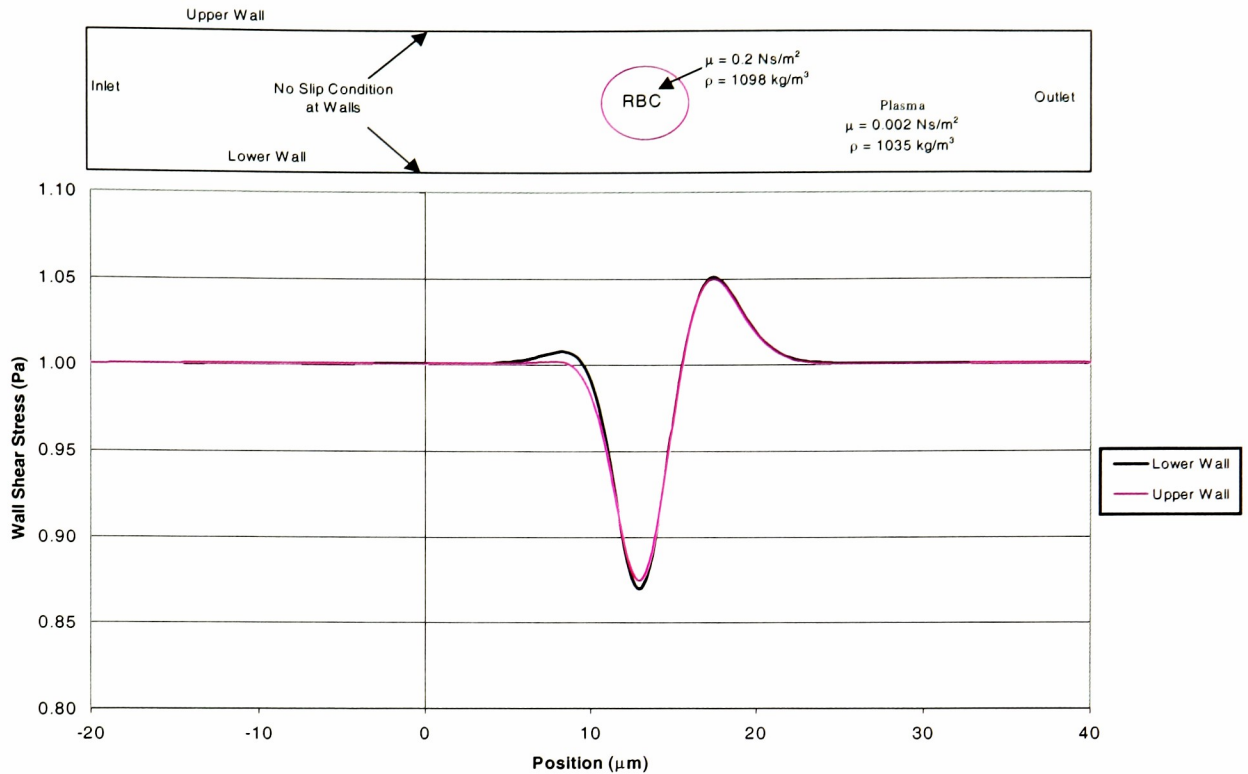


Figure 3.17: Wall Shear Stress, Droplet Flow

3.3.2

Analysis of Droplet Property Values in a 30 Degree Bifurcation

Varying surface tension values and viscosity values separately, analysis results of droplet behavior within the region of the bifurcating flow was then compiled to determine corresponding effect on droplet shape (Figures 3.18 and 3.19). Both Figures 3.18 and 3.19 show Pressure Contour Plots directly from FIDAP that show the droplet shape in the flow near the apex. Each Figure shows results from a series of analysis reflecting five different values for the corresponding property being analyzed.

It's important to note here that the compiled data of defining properties of human blood and its constituents shown earlier in the presentation of background research was

not directly applicable in the following studies since property values within the hamster circulatory system to which these results were compared differ. However, these compiled values gave a starting point from which to set defining properties within the computational model. The ability of these defining properties to maintain an appropriate circular droplet shape while varying starting position (non-centered between the vessel walls) was also studied. The fluid viscosity values are presented as λ , a ratio of droplet viscosity to plasma viscosity. Fluid surface tension values are represented by surface tension, σ .

The range of droplet viscosity values was chosen high under the intuition that a solid particle would effectively behave the same as a fluid droplet of infinitely high viscosity, considering the droplet alone. In considering the behavior of a droplet in a flow, similar intuition was used in choosing fluid surface tension values. Use of surface tension values greater than 1.0E-05 Pa is not recommended for flow analysis since the convergence of the solution becomes more computationally intense. As these are transient analyses, when defining fluid surface tension values greater than 1.0E-05 Pa, the size of the time step required to achieve desired flow solution convergence becomes several orders of magnitude smaller than that required for analysis using surface tension values less than 1.0E-05. Thus, greater computational time is needed to achieve the solution of the flow of the droplet through the entire flow domain defined by the bifurcation model. Furthermore, analysis of the flow results using $\sigma=1.0E-05$ Pa revealed a droplet translation velocity slower than the other cases analyzed, which disqualified these values as appropriate to characterizing accurate RBC flow behavior.

With increasing droplet viscosity, increasing droplet rigidity was observed (Figure 3.18). In comparison to the effect of viscosity on droplet shape, a similar, but larger trend of increasing droplet rigidity with increasing surface tension values was shown (Figure 3.19). For surface tension values below $1.0\text{E-}07$ Pa, the droplet breaks apart in the region of the bifurcation. For values between $1.0\text{e-}07$ Pa and $1.0\text{e-}06$ Pa, no droplet breakage was observed and no excessive computational time was required for flow solution, making these surface tension values most appropriate for further flow studies. Observations from varying each defining property, viscosity and surface tension, are important, however, incomplete, since the influence, if any, on wall shear stress is still unknown. The research addressing this determining factor is presented in the next section.

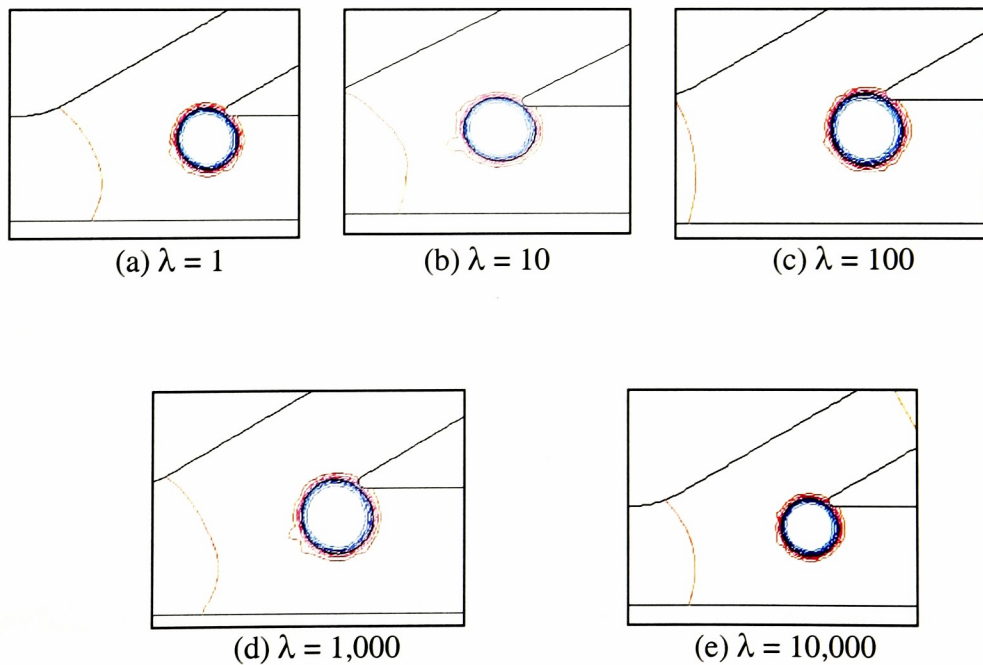


Figure 3.18a-e: Droplet Behavior with Changing Viscosity

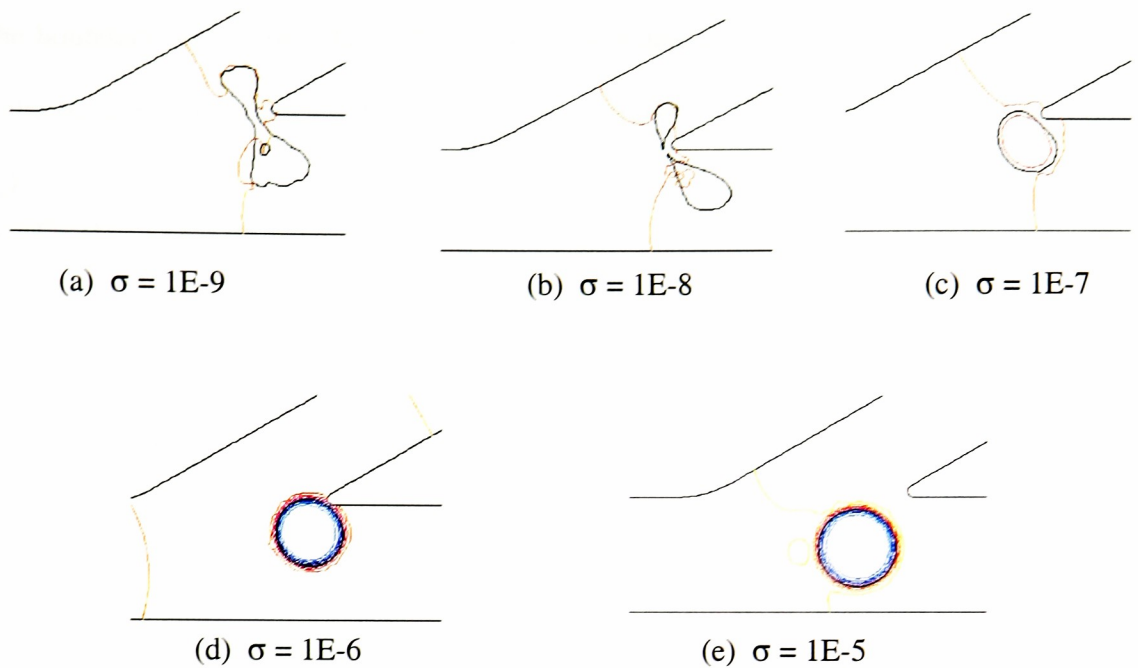


Figure 3.19a-e: Droplet Behavior with Changing Surface Tension

All computational analyses of droplet flow to this point have initialized with the droplet centered at the inlet between the vessel walls. The effect of varying the starting location of the droplet was investigated in straight vessel geometry for simplicity. The initial goal was to determine the droplet behavior and then the correlation, if any, between the initialized starting location of the droplet and the flow path through a bifurcating geometry, branch vessel or parent vessel. Following the computational methodology developed in this research, the droplet, when initialized off-center between the vessel walls, did not maintain an appropriate circular shape. In addition, as RBCs have been observed to rotate while translating through vessels, duplication of this flow characteristic is not possible using the VOF model. By the definition of the fluid continuity conserved with this numerical technique, the flow across the fluid interface between the droplet and plasma fluid must be continuous, therefore limiting rotation as a

possible droplet flow behavior in this research. In all cases, the shear forces developed by the boundary layer along the walls of the computational domain were much stronger than the surface tension force holding the droplet together.

3.3.3 Qualification of Droplet Property Values

With droplet property values determined to capture appropriate physical behavior, influence on wall shear stress behavior was characterized to confirm the accuracy of the modeling approach prediction capabilities. In analyzing results of the droplet-laden flows, it was necessary to isolate droplet viscosity and fluid surface tension and examine their respective influence on the characteristic of the wall shear stress reverse s-curve pattern.

A comparison of wall shear stress from analyses with varying viscosity shows a dependency on wall shear stress (Figure 3.20). The local maximum and minimum increase by as much as 25% with increasing droplet viscosity.

RBC Droplet Viscosity Effect on Wall Shear Stress*
 Straight Vessel, Single RBC Droplet, 2D, Re = 0.01, $\sigma = 1.0226E-06$

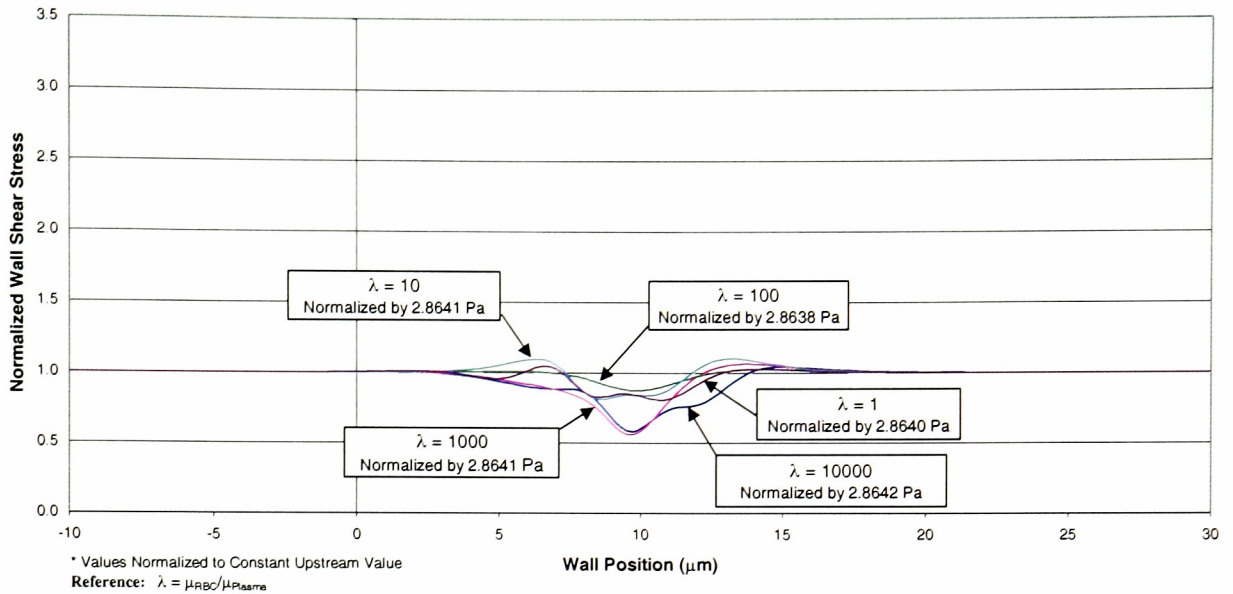


Figure 3.20: Wall Shear Stress Dependency on Droplet Viscosity

In a similar manner, observing the dependency of the fluid surface tension value the characteristic “s” wall shear stress pattern is observed, however, with a much greater variance in magnitude than from increasing viscosity (Figure 3.21). In comparison to droplet viscosity influence on wall shear stress, surface tension is shown to have a larger influence on wall shear stress with decreases in local minima of 40% and increases in local maxima of 350% ($\sigma=1.0E-05$ Pa). This large influence on wall shear stress is expected for high, surface tension driven flows, however, analysis was needed to determine the point at which the transition between viscous driven flow and surface tension driven flow occurs.

Fluid Surface Tension Effect on Wall Shear Stress*
 Straight Vessel, Single RBC Droplet, 2D, $Re = 0.01$, $\lambda = 100$ **

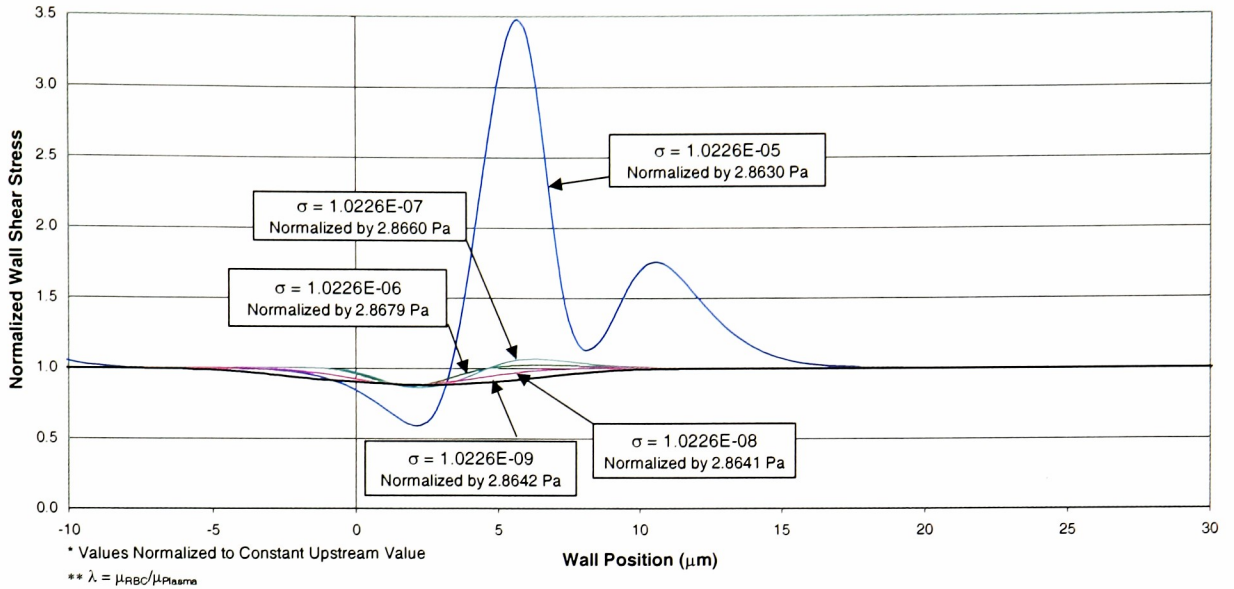


Figure 3.21: Wall Shear Stress Dependency on Surface Tension

In summary, computational predictions suggest the presence of a red blood cell in plasma flow in the microcirculation has a substantial effect on the wall shear stress distribution, causing a characteristic s-curve shape. The credibility of these findings is supported by other research findings of flattened transverse velocity profiles in microcirculatory vessels (Bishop, J. J. et al., 2001, Lerche, D. and Oelke, R., 1990, Sugii et al., 2002). This investigation has also explored the influence of droplet viscosity and fluid surface tension as new factors influencing wall shear stress, introduced by the volume of fluid modeling technique used to approximate the translation of a solid particle in a flow with the translation of a fluid droplet in a flow.

3.3.4 Droplet Presence in a Bifurcation

With a more complete understanding of the property definitions needed for analysis of droplet flow, the droplet influence on wall shear stress in a bifurcation was investigated in its entirety.

The flow characteristics of droplet presence in a 30 degree bifurcation was studied. The bifurcation geometry included a $10\mu\text{m}$ branch radius and a $1\mu\text{m}$ apex radius. For each wall, upper front (Figure 3.23), upper back (Figure 3.24), and lower (Figure 3.25), wall shear stress characterizations are shown for five positions of the droplet as it translated through the bifurcation geometry (Fig. 3.22). Each droplet color shown in the graph correlates to a different position in time and therefore, a different location within the bifurcation geometry. These wall shear stress values were again normalized to a constant upstream shear stress value for comparison purposes.

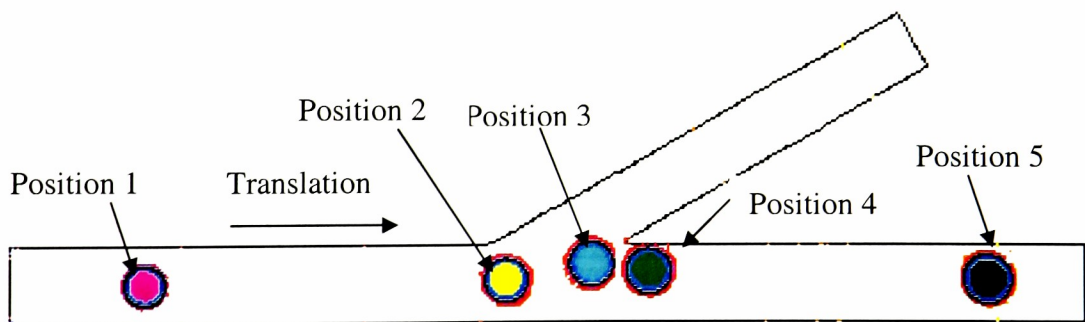
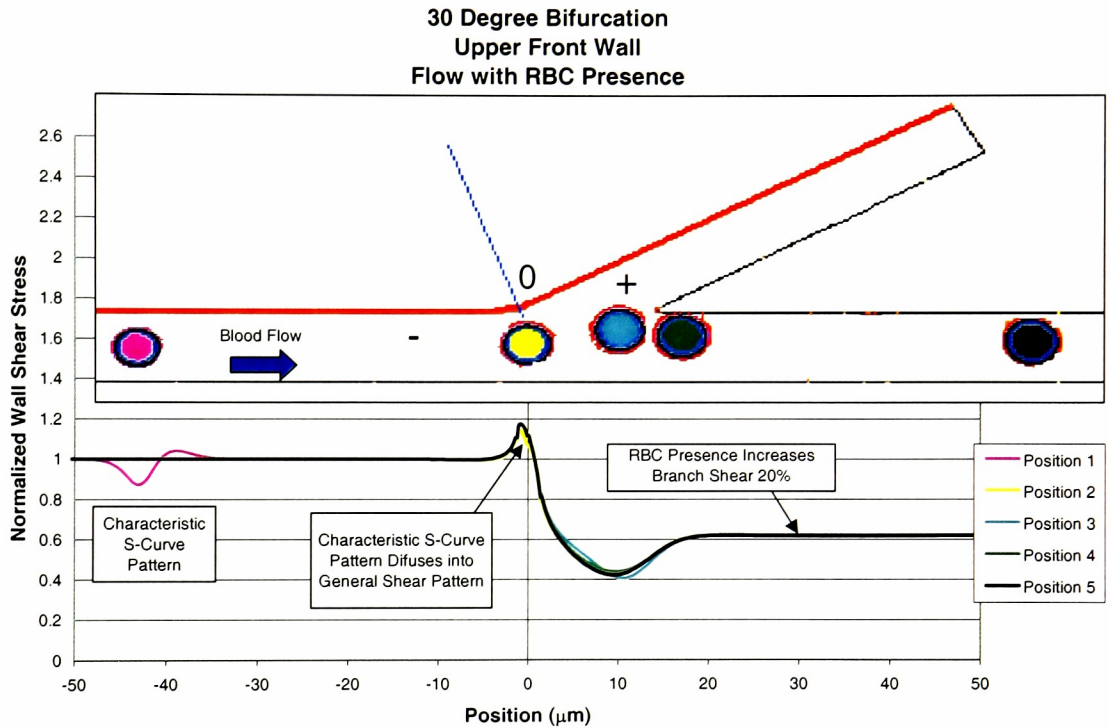


Figure 3.22: Bifurcation Geometry with Droplet Position

Along the upper front wall, the characteristic s curve presented first in the straight channel studies is also apparent in the bifurcation study at each of the five positions (Fig. 3.23). The wall shear stress trend caused by the droplet presence is shown to compliment

the general shear pattern characteristic for a bifurcation. The Magnitudes of the maximum and minimum shear in the s curve pattern from this analysis, 1.05 and 0.90 respectively, are equivalent to the magnitudes found in the straight channel analysis. The general drop in wall shear stress is nearly 40%, in the parent vessel outlet segment.



3.23: Droplet Presence in a Bifurcation, Upper Front Wall Normalized Wall Shear Stress

Wall shear signature along the upper back wall reveals a characteristic s curve in the branch and flow distribution effects consistent with those along the upper front wall (Fig. 3.24). The s-curve shape disturbance in wall shear is caused by the droplet presence at position five near the exit of the flow model. The magnitudes of the pattern are again consistent with the patterns found along the upper front wall and in the straight vessel

analysis. Furthermore, the normalized wall shear stress shown for the outlet vessel segment is nearly 0.6, which is in agreement with the results along the upper front wall.

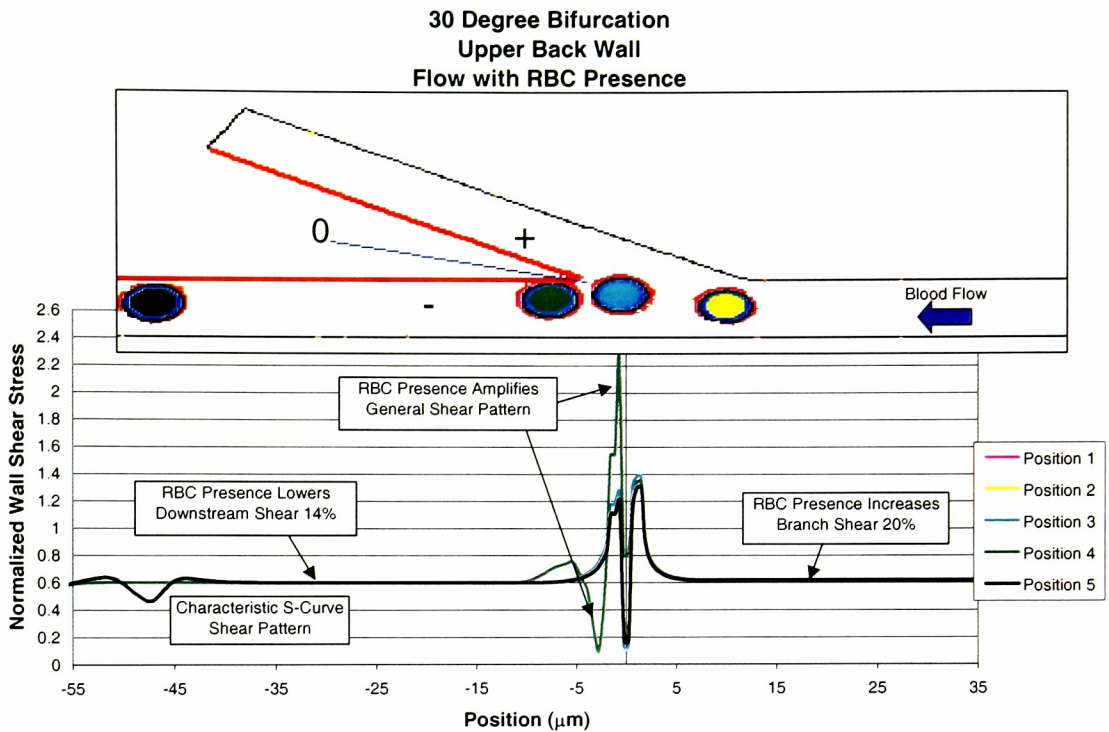


Figure 3.24: Droplet Presence in a Bifurcation, Upper Back Wall Normalized Wall Shear Stress

Analysis results along the lower bifurcation wall show trends consistent with those shown along the upper front wall and upper back wall. The wall characterization reveals the same cumulative effects caused by the general bifurcation trend and the droplet presence. Also, the general changes in normalized wall shear stress, from 1.0 and 0.6, inlet segment to parent outlet segment respectively, are in agreement with the observations along the other two walls.

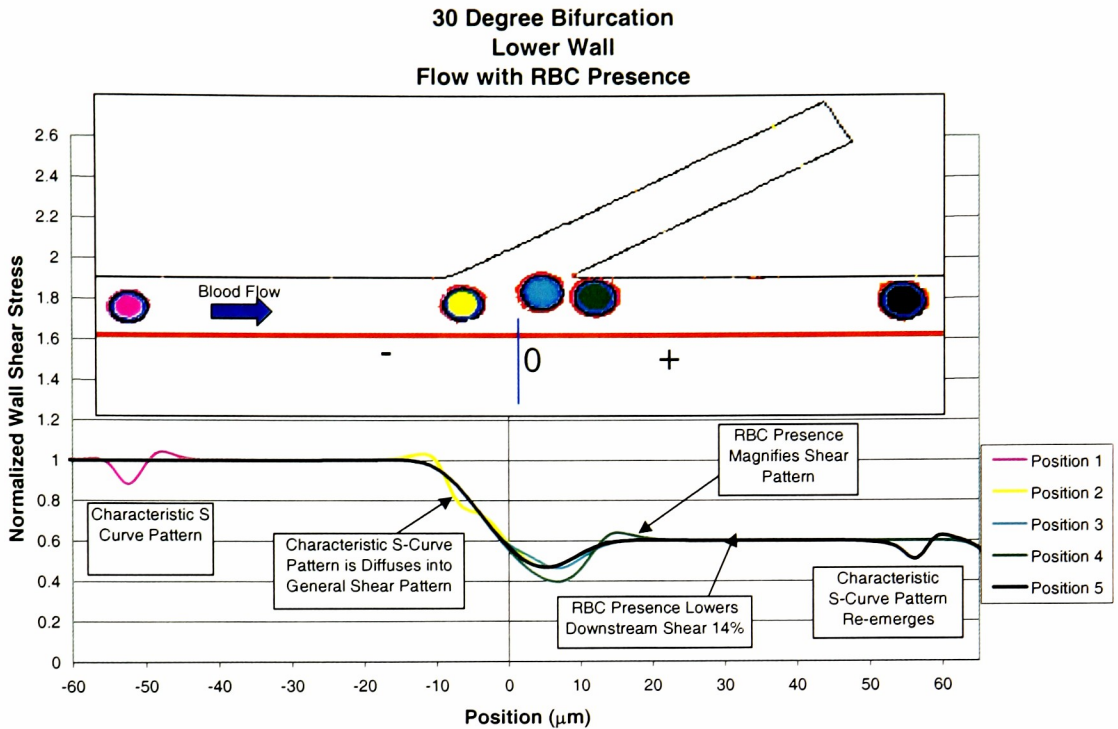


Figure 3.25: Droplet Presence in a Bifurcation, Lower Wall Normalized Wall Shear Stress

Particle presence in arteriolar bifurcation flow is shown to have a significant influence on wall shear stress characterizations. The influence observed is a localized flow disturbance caused directly by the presence of the droplet overlaid with the typical wall shear stress distribution shown for a bifurcating flow domain.

The integrity of the computation model is proven by consistency in wall shear rates along the three walls of the bifurcation geometry and the characteristic s-curve pattern on the wall adjacent to the droplet location, equivalent in magnitude to that given by the straight vessel analysis.

3.3.5

Multiple Droplets in a Flow

The final segment of research focused on the consideration of modeling blood Hematocrit by modeling a number of droplets in a flow. Specifically, this investigation sought to characterize the wall shear stress influence of two surrounding droplets on the characteristic s-curve shear pattern shown by the earlier results of the straight and bifurcating vessel geometries. Dr. Frame prescribed the spacing between the fluid droplets as one droplet diameter. Staying consistent with all results presented in this research, all values were normalized to a constant wall shear stress value for comparison purposes.

With the influence of a single droplet in a flow on wall shear stress characterized, the effect of two surrounding droplets on the same characteristic was studied. Consistently, the characteristic s-shape is apparent for each droplet, with the local minima directly adjacent to the droplet position and a small local maximum directly upstream (Fig. 3.26). The local minimum in wall shear stress is shown most pronounced for the leading droplet, which blocks the flow creating a flattened velocity profile. However, the respective local minimum is least pronounced for the middle droplet, which indicates a channeling effect of the flow around the droplets along the vessel walls creating an increased near-wall flow velocity. This effect is seen for the trailing droplet as well, as the local respective wall shear stress minimum is still larger than that of the leading droplet.

In addition to the characteristic s-curve pattern, there is a second local maximum, directly downstream of each droplet position. A local maximum 10% higher than those

upstream of each droplet position is most pronounced for the middle droplet. For the surrounding two droplets, the maximum is nearly 5% higher than the maxima upstream of the droplet locations. This variation is also attributed to the channeling effect of the flow around the droplets along the vessel wall again creating a higher velocity near the wall. As a result of these additional local maxima downstream of each droplet position, the wall shear stress between the droplets is temporally increased.

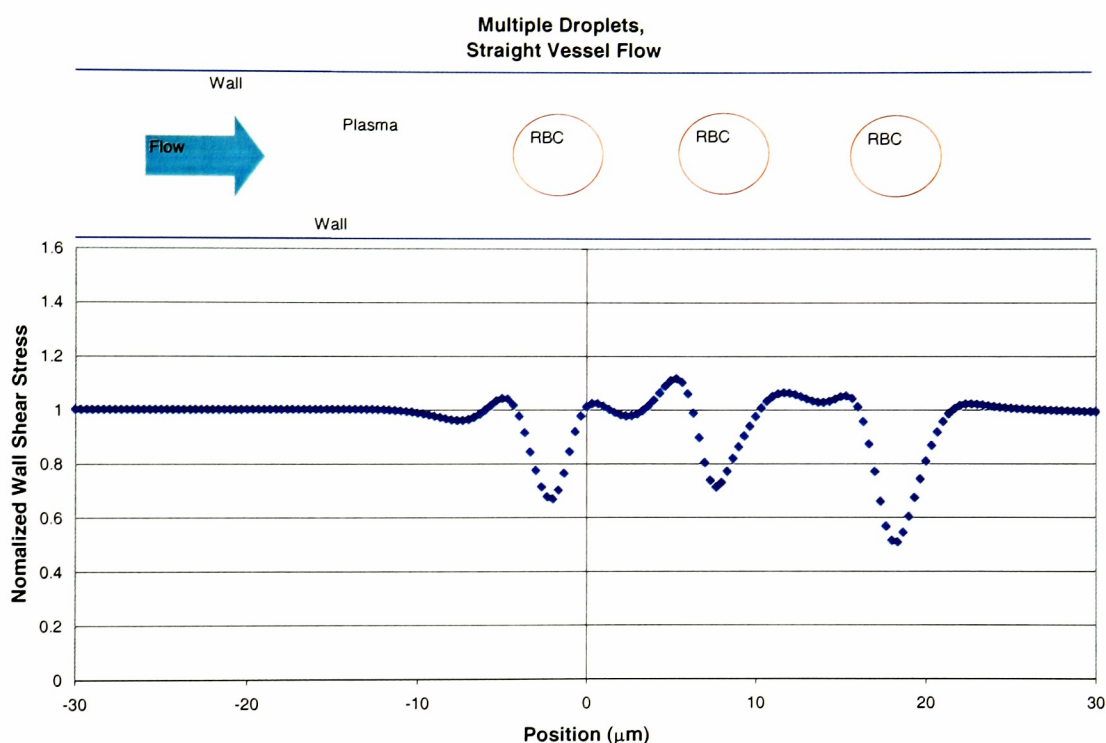


Figure 3.26: Multiple Droplets in Straight Vessel, Normalized Wall Shear Stress

The flow behavior of multiple droplet flow in a 30 degree bifurcation was also studied, however, with unfortunate results. The model was unable to predict appropriate translational characteristics of a particle laden flow through a bifurcation. When approaching the bifurcating region of the fluid domain, the droplets coalesce into a larger droplet. This combining behavior shown by the individual droplets would otherwise

represent the collision of solid RBC particles. Since the particles are approximated as fluid droplets, they are unable to collide, and instead combine. In addition, the coalescing behavior is enhanced by the defining fluid surface tension characteristic needed to maintain appropriate circular shape of a single droplet. The flow obstruction presented by the apex forces the droplets into closer proximity to one another where the surface tension forces, which seek to minimize the surface area of the droplet fluid, cause the three individual droplets to unite to form a single larger droplet.

Reviewing this investigation, the research developed a consistent computational modeling approach to characterize the effect of RBC presence on wall shear stress. In doing so, the implications of approximating erythrocyte presence with fluid droplet presence and the development of a multi-droplet method, accounting for blood Hematocrit, was also studied.

The investigation of the influence of droplet presence on wall shear stress revealed a characteristic s-shaped pattern that was equivalent in magnitude when studied in straight and bifurcating vessels. To prove appropriate RBC behavior, this study included observation of the droplet shape while translating through the vessel. This was done using a bifurcating vessel since the apex region of the fluid domain presented a passive flow obstruction to prove the droplet behavior. It was in this study that the defining properties of a fluid droplet that directly relate to its flow behavior and shape, surface tension and viscosity, were varied.

Remaining consistent with the goal of this analysis to determine and quantify the wall shear stress effect caused by the presence of RBC's in a flow, the effect of the

defining surface tension and viscosity properties of the droplet was also investigated individually. These analyses revealed a positive correlation between each fluid property and wall shear stress. Either an increase in droplet viscosity or an increase in surface tension resulted in an increase in the magnitudes of the local extrema of the characteristic shear stress pattern, with surface tension having a much larger effect than that of viscosity. Although the property definitions of viscosity and surface tension were found to influence wall shear stress, their effect was quantified.

To carry the examination of the influence of RBC presence on wall shear stress in microvascular flow further, the effect of three droplets in a flow was studied. The primary result of this study was to quantify the effect of two surrounding droplets on the localized wall shear stress pattern characteristic of a single droplet.

Chapter 4

Future Developments

The intent of this paper was to improve the development of an accurate and efficient process of characterizing wall shear properties in arteriolar bifurcations via computational techniques. Despite study of the influence of bifurcation corner geometry and particle presence on flow properties, other factors such as wall compliance, wall slip effects caused by the glycocalyx lining the vessels, and surfactants on the surface of RBC's are newly studied characteristics of blood flow in arteriolar vessels whose impact on flow properties may now be investigated computationally, using the methodology developed in this research.

Journal of Biomechanical Engineering

4.1

Appropriateness of Study Simplifications

In consideration for the added complexity of the arteriolar bifurcation model characteristics, simplifications were made in a fashion to determine effects of corner geometry and RBC presence singularly. The typical analysis methodology of investigating Newtonian flow in arteriolar network was used as a baseline for comparisons made in this research. Although the simplification of a two-dimensional flow influences wall shear stress values, the effect is fully quantified and may be incorporated as a correction to analysis results.

The approach taken by this research isolated different factors involved in the computational modeling methodology as possible influences to wall shear stress characteristic and presented comparisons to currently accepted results in an effort to

quantify their relative effect on wall shear stress. Accordingly, factors such as wall compliance, glycocalyx, and surfactants may be evaluated in this same manor, which offers the achievability of quantified results that are efficiently obtainable with current available technology and that may be shown as a conglomerate to depict more accurately the wall shear stress characterizations within the arteriolar networks.

4.1.1 2-D Simplification

The agreeable comparison between the normalized three-dimensional and two-dimensional flow studies establishes the simplified, two-dimensional approach as credible. Looking a step further, a “characteristic” constant, upstream wall shear stress value may be used to map the normalized two-dimensional values to realistic three-dimensional quantities in situations where the real wall shear stress values are desired.

4.1.2 Volume of Fluid

For the analysis of RBC presence in plasma, the Volume of Fluid method offers a possible alternative to studying the particulate nature of blood and the corresponding influence on wall shear stress. The conclusions from this research do show the significance of addressing the RBC presence in determining wall shear stress. However, the accuracy of the results, being dependent on fluid properties of the droplet aren't entirely characteristic of RBC's. The characterization of the solid properties of the RBC gives the best representation of the actual physical flow rheology, although the numerical intensity and ingenuity required in solving such a problem is surpasses the capabilities of this research.

4.2

Multi-Particle Simulations

The investigations presented in this study present an accurate method of modeling the presence of multiple droplet particles in microvascular flow, however limited to a straight vessel geometry. The methodology developed in this study may be used as a basis for further wall shear stress characterization of multiple droplet presence in a flow as an accurate representation of blood Hematocrit.

4.3

Three-Dimensional Model

Upon reaching an efficient level in resolving the computational complexities of large solid particle movement in a flow, additional flow factors resulting from the three-dimensional flow domain may be further analyzed and included for a complete correction of wall shear stress associated within the vasculature of the microcirculation. As available computational technology evolves further, the modeling of finite segments of the arteriolar network will progress into models of entire network flow fields, giving greater understanding to the autoregulatory mechanics stimulated by flow characteristics as they relate to responses present in the microcirculatory system.

REFERENCES

- Barbenel, J. C. 1981. The Measurement of Red Blood Cell Deformability. In *Clinical Aspects of Blood Viscosity and Cell Deformability*, G.D.O. Lowe, J. C. Barbenel, C.C. Forbes, Eds., Springer-Verlag, Berlin Heidelberg, New York. Pp. 37-45.
- Bishop, J. J. et al. 2001. Effect of erythrocyte aggregation on velocity profiles in venules. *Am J Physiol Heart Circ Physiol* 280: H222-H236.
- Cassot, F., Lorthois, S., and Zagoule, M. 1998. Microvascular networks. In *Intra and Extracorporeal Cardiovascular Fluid Dynamics, Vol. 1-General Principles in Application*, P. Verdonck, Ed., Computational Mechanics Publications, Boston, 77-100.
- Damiano, E. R. 1998. The Effect of the Endothelial-Cell Glycocalyx on the Motion of Red Blood Cells through Capillaries. *Microvascular Research* 55: 77-91.
- Evans, E. A. and Yeung, 1989. Apparent viscosity and cortical tension of blood granulocytes determined by micropipette aspiration. *Biophys J* 56(1): 151-160.
- Evans, E. A., Waugh, R. E., and Melnik, L. 1976. ELASTIC AREA COMPRESSIBILITY MODULUS OF RED CELL MEMBRANE. *Biophys J* 16: 585-595.
- Fluent, Inc. FIDAP 8.6.2 Documentation. CD-ROM. New Hampshire: Lebanon, 2001.
- ¹Fox, R. J. and Frame, M. D. 2002. Arteriolar Flow Recruitment with Vitronectin Receptor Stimulation Linked to Remote Wall Shear Stress. *Microvascular Research* 64: 414-424.
- ²Fox, R. J. and Frame, M. D. 2002. Regulation of flow and wall shear stress in arteriolar networks of the hamster cheek pouch. *J Appl Physiol* 92: 2080-2088.
- Frame, M. D. and Sarelius, I. H. 1996. Endothelial cell dilatatory pathways link flow and wall shear stress in an intact arteriolar network. *J Appl Physiol* 81(5): 2105-2114.
- Frame, M. D. and Sarelius, I. H. 1993. Arteriolar Bifurcation Angles Vary with Position and When Flow is Changed. *Microvascular Research* 46: 190-205.
- Frame et al. 1998. Shear Stress gradient over endothelial cells in a curved microchannel system. *Biorheology* 35(4): 245-261.
- Golster, H. et al. 1999. TECHNICAL REPORT: Red Blood Cell Velocity and Volumetric Flow Assessment by Enhanced High-Resolution Laser Doppler Imaging in Separate Vessels of the Hamster Cheek Pouch Microcirculation. *Microvascular Research* 58: 62-73.

- Harkness, J. 1971. The viscosity of human blood plasma; its measurement in health and disease. *Biorheology* Dec; 8(3): 171-193.
- Hochmuth, R. M. 2000. Micropipette aspiration of living cells. *J of Biomech* 33: 15-22.
- Hochmuth, R. M. 1987. Properties of Red Blood Cells. In *Handbook of Bioengineering*, R. Skalak and S. Chien, Eds., McGraw-Hill, New York, 12.1-12.17.
- Katnik, C. and Waugh, R. E. 1990. Alterations of the apparent area expansivity modulus of red blood cell membrane by electric fields. *Biophys J* 57(4): 877-882.
- Kiani, M. F. and Cokelet, G. R. 1994. Additional Pressure Drop at a Bifurcation Due to the Passage of Flexible Disks in a Large Scale Model. *J Biomech Eng.* 116(11): 497-501.
- Kim, M. B. and Sarelius, I. H. 2003. Distributions of Wall Shear Stress in Venular Convergences of Mouse Cremaster Muscle. *Microcirculation* 8: 167-178.
- Lerche, D. and Oelke, R. 1990. Theoretical model of blood flow through hollow fibres considering hematocrit-dependent, non-Newtonian blood properties. *The International Journal of Artificial Organs* 13(11): 742-746.
- Lipowski, H. H. 1987. Mechanics of Blood Flow in the Microcirculation. In *Handbook of Bioengineering*, R. Skalak and S. Chien, Eds., McGraw-Hill, New York, 18.1-18.25.
- Lominadze, D. and Mchedlishvili, G. 1999. Red Blood Cell Behavior at Low Flow Rate in Microvessels. *Microvascular Research* 58: 187-189.
- Misra, J. C., Patra, M. K., and Misra, S. S. 1993. Biorheological Aspects of Arterial Flow near Bifurcations. *Computers Math. Applic.* 26(9): 53-65.
- Noren, D. A Study of Fluid Flow through Arteriolar Bifurcations: Computational and In Vivo Comparison. Thesis. U of Rochester, 1999. U of Rochester: Rochester, 1999.
- Popel, A. S. and Pittman, R. N. 2000. Mechanics and Transport in the Microcirculation. In *The Biomedical Engineering Handbook, 2nd ed., Vol. 1*, J. D. Bronzino, Ed., CRC Press and IEEE Press, Boca Raton, 31.1-31.12.
- Pries et al. 1997. Microvascular blood flow resistance: role of endothelial surface layer. *Heart and Circulatory Physiology* 273(5).
- Pries et al. 1990. Blood flow in microvascular networks. *Circulation Research* 67: 826-834.
- Schneck, D. J. 2000. An Outline of Cardiovascular Structure and Function. In *The Biomedical Engineering Handbook, 2nd ed., Vol. 1*, J. D. Bronzino, Ed., CRC Press and IEEE Press, Boca Raton, 1.1-1.12.

- Sugii, Y., Nishio, S., and Okamoto, K. 2002. *In vivo* PIV measurement of red blood cell velocity field in microvessels considering mesentery motion. *Physiol. Measurement* 23: 403-416.
- Taylor C. A. 2000. Finite element modeling of blood flow: Relevance to Atherosclerosis. In *Intra and Extracorporeal Cardiovascular Fluid Dynamics, Vol. 2-Fluid Structure Interaction*, P. Verdonck and K. Perktold, Eds., WIT Press, Boston, 249-290.
- Waugh, R. E. and Evans, E. A. 1979. Thermoelasticity of Red Cell Membrane. *Biophys J* 26(4): 115-132.
- Waugh, R. E. and Hochmuth, R. M. 2000. In *The Biomedical Engineering Handbook, 2nd ed., Vol. 1*, J. D. Bronzino, Ed., CRC Press and IEEE Press, Boca Raton, 32.1-32.13.
- Zapryanov, Z., Tabakova, S. *Dynamics of Bubbles, Drops, and Rigid Particles*. Kluwer Academic Publishers. Norwell, MA. 1999.
- Zhao et al. 2000. Blood flow and vessel mechanics in a physiologically realistic model of a human carotid arterial bifurcation. *J Biomechanics* 33(8): 975-984.

A1

Newtonian Flow, Corner Geometry Analysis, Bifurcation Size

Bifurcation Angle	Branch Radius (μm)	Apex Radius (μm)	Bifurcation Size (μm)
30 Degrees	10	sharp	16.00
	10	1	16.53
	10	2	17.00
	sharp	1	16.00
	5	1	16.50
	10	1	16.53
90 Degrees	sharp	sharp	8.00
	5	5	8.00
	10	10	8.00
150 Degrees	sharp	10	16.00
	1	10	16.53
	2	10	17.00
	1	sharp	16.00
	1	5	16.50
	1	10	16.53

*Bifurcation Size is Characterized by Shortest Horizontal Line Crossing Bifurcation Region of Geometry

A2

Analysis Shortcomings

Three Dimensional Mesh: The three dimensional bifurcation geometry was meshed using a tetrahedral meshing scheme using Gambit 2.0. Use of a hexahedral meshing scheme is ideal, however, application of these schemes in Gambit will require great skill.

Droplet Surface Tension Values: For surface tension values larger than $1E-05$, the transient flow solution took days to obtain as opposed to one day for values less than $1E-05$. From the results, the approximate droplet translational velocity was noticeably slower than in flow solutions using surface tension values less than $1E-05$. This confirms a turning point in the overall flow characteristics (the surface tension forces are beginning to compete with the viscous forces of flow). In this study, the approximation of a solid particle in a flow by a fluid droplet in a flow only attempts to use surface tension forces in a "passive" sense to hold the droplet together in spherical (circular) shape. The viscous forces of the flow on the particle remain the primary driving force causing the translation.

Guidelines for Continuation of Research

Computational Accuracy: Analysis may be done to further validate the computational accuracy of the results presented here.

Flow Split: Since the flow split may not be pre-defined for the particle analyses using FIDAP 8, a baseline should be established with Newtonian flow, no droplet. This

baseline would serve to compare with droplet analysis results and reveal flow blockage effects causing fluctuations in flow split.

Corner Geometry File Name Convention: Each bifurcation angle is denoted by "B30," "B90," and "B150." The file names give the corresponding acute angle radius, "a0.1" followed by the obtuse angle radius, "o1.0."

FIDAP Read Files: For the FIDAP analyses, the computational domain was developed using Gambit 2.0. A corresponding .FDREAD file was constructed in NOTEPAD to simplify analysis set-up in FIDAP. Correct use of this file will make save a tremendous amount of analysis set up time. All analysis conditions may be specified using commands written in FIDAP syntax. As the model characteristics change, a previous .FDREAD file may be modified for use as many of the commands are duplicated.